



1 **Objective Evaluation of Earth System Models: PCMDI Metrics Package**  
2 **(PMP) version 3**

3

4 Jiwoo Lee<sup>1</sup>, Peter J. Gleckler<sup>1</sup>, Min-Seop Ahn<sup>2,3</sup>, Ana Ordonez<sup>1</sup>, Paul A. Ullrich<sup>1,4</sup>, Kenneth R.  
5 Sperber<sup>1,a</sup>, Karl E. Taylor<sup>1</sup>, Yann Y. Planton<sup>5,6</sup>, Eric Guilyardi<sup>7,8</sup>, Paul Durack<sup>1</sup>, Celine Bonfils<sup>1</sup>,  
6 Mark D. Zelinka<sup>1</sup>, Li-Wei Chao<sup>1</sup>, Bo Dong<sup>1</sup>, Charles Doutriaux<sup>1</sup>, Chengzhu Zhang<sup>1</sup>, Tom Vo<sup>1</sup>,  
7 Jason Boutte<sup>1</sup>, Michael F. Wehner<sup>9</sup>, Angeline G. Pendergrass<sup>10,11</sup>, Daehyun Kim<sup>12</sup>, Zeyu Xue<sup>13</sup>,  
8 Andrew T. Wittenberg<sup>14</sup>, and John Krasting<sup>14</sup>

9

10 <sup>1</sup> Lawrence Livermore National Laboratory, Livermore, California, USA

11 <sup>2</sup> NASA Goddard Space Flight Center, Greenbelt, MD, USA

12 <sup>3</sup> ESSIC, University of Maryland, College Park, MD, USA

13 <sup>4</sup> University of California, Davis, Davis, California, USA

14 <sup>5</sup> NOAA Pacific Marine Environmental Laboratory, Seattle, Washington, USA

15 <sup>6</sup> Monash University, Clayton, Australia

16 <sup>7</sup> LOCEAN-IPSL, CNRS-IRD-MNHN-Sorbonne Université, Paris, France

17 <sup>8</sup> National Centre for Atmospheric Science-Climate, University of Reading, Reading, UK

18 <sup>9</sup> Lawrence Berkeley National Laboratory, Berkeley, California, USA

19 <sup>10</sup> Department of Earth and Atmospheric Science, Cornell University, Ithaca, New York, USA

20 <sup>11</sup> National Center for Atmospheric Research, Boulder, Colorado, USA

21 <sup>12</sup> School of Earth and Environmental Sciences, Seoul National University, Seoul, South Korea

22 <sup>13</sup> Pacific Northwest National Laboratory, Richland, WA, USA

23 <sup>14</sup> NOAA Geophysical Fluid Dynamics Laboratory, Princeton, NJ, USA

24 <sup>a</sup> Retired

25

26

27

28

29 *Corresponding to:* Jiwoo Lee ([lee1043@llnl.gov](mailto:lee1043@llnl.gov))

30 7000 East Ave, Livermore, California 94550, USA



31 **Abstract**

32

33 Systematic, routine, and comprehensive evaluation of Earth System Models (ESMs) facilitates benchmarking  
34 improvement across model generations and identifying the strengths and weaknesses of different model  
35 configurations. By gauging the consistency between models and observations, this endeavor is becoming increasingly  
36 necessary to objectively synthesize thousands of simulations contributed to the Coupled Model Intercomparison  
37 Project (CMIP) to date. The PCMDI Metrics Package (PMP) is an open-source Python software package that provides  
38 "quick-look" objective comparisons of ESMs with one another and with observations. The comparisons include  
39 metrics of large- to global-scale climatologies, tropical inter-annual and intra-seasonal variability modes such as El  
40 Niño-Southern Oscillation (ENSO) and Madden-Julian Oscillation (MJO), extratropical modes of variability, regional  
41 monsoons, cloud radiative feedbacks, and high-frequency characteristics of simulated precipitation, including  
42 extremes. The PMP results are produced in the context of all model simulations contributed to CMIP6 and earlier  
43 CMIP phases. An important priority of the PMP is to document evaluation statistics for all Historical and AMIP  
44 simulations submitted to recent phases of CMIP, providing version-controlled information for all data sets and  
45 software packages being used. Among other purposes, this also enables modeling groups to assess performance  
46 changes during the ESM development cycle in the context of the error distribution of the multi-model ensemble. In  
47 this paper, we present an overview of the PMP including its history to date, capabilities, recent updates, and future  
48 direction.



## 49 **1 Introduction**

50 Earth System Models (ESMs) are key tools for projecting climate change and conducting research to enhance our  
51 understanding of the Earth system. Enhancing the reliability of models is therefore important, yet evaluating ESMs is  
52 a complex endeavor, given the vast range of climate characteristics across space and time scales. A necessary step to  
53 evaluate the performance of ESMs is quantifying their consistency with available observations.

54 The Program for Climate Model Diagnosis and Intercomparison (PCMDI) has worked closely with the World  
55 Climate Research Programme's (WCRP) Working Group on Coupled Models (WGCM) and Working Group on  
56 Numerical Experimentation (WGNE) to design and support Model Intercomparison Projects (MIPs) (Potter et al.,  
57 2011). This effort began with the Atmospheric Model Intercomparison Project (AMIP; Gates, 1992; Gates et al.,  
58 1999), and has continued through multiple phases of the Coupled Model Intercomparison Project (CMIP; Meehl et  
59 al., 1997, 2000, 2007; Covey et al., 2003; Taylor et al., 2012). The most recent phase of CMIP (CMIP6; Eyring et al.,  
60 2016) provides a set of well-defined experiments that most climate modeling centers perform, and subsequently makes  
61 results available for a large and diverse community to analyze.

62 Climate model performance metrics have been widely used to objectively and quantitatively gauge the  
63 agreement between observations and simulations to summarize model behavior in a wide range of model evaluations.  
64 Simple examples include either the model bias or the pattern similarity (correlation) between an observed and  
65 simulated field (e.g., Taylor, 2001). With the rapid growth in the number, scale, and complexity of simulations, the  
66 metrics have been used more routinely as exemplified by the Intergovernmental Panel on Climate Change (IPCC)  
67 Assessment Reports (e.g., Gates et al., 1995; McAvaney et al., 2001; Randall et al., 2007; Flato et al., 2014; Eyring et  
68 al., 2021). A few studies have been exclusively devoted to objective model performance assessment using summary  
69 statistics. Lambert and Boer (2001) evaluated the first set of CMIP models from CMIP1 using statistics for the large-  
70 scale mean climate. Gleckler et al. (2008) identified a variety of factors relevant to model metrics and demonstrated  
71 techniques to quantify the relative strengths and weaknesses of the simulated mean climate. Reichler and Kim (2008)  
72 attempted to gauge model improvements across the early phases of CMIP. The scope of objective model evaluation  
73 has greatly broadened beyond the mean state in recent years (e.g., Gleckler et al., 2016; Eyring et al., 2019), including  
74 attempts to establish performance metrics for a wide range of climate variability (e.g., Kim et al., 2009; Sperber et al.,  
75 2013; Ahn et al., 2017; Fasullo et al., 2020; Lee et al., 2021b; Planton et al., 2021) and extremes (e.g., Sillmann et al.,  
76 2013; Srivastava et al., 2020; Wehner et al., 2020, 2021). Guilyardi et al. (2009) and Reed et al. (2022) emphasized  
77 that metrics should be concise, interpretable, informative, and intuitive.

78 Considering the exponential growth of data size and diversity of ESM simulations, there has been a pressing  
79 need for the research community to become more efficient and systematic in evaluating ESMs and documenting their  
80 performances. To respond to the need, PCMDI has developed the PCMDI Metrics Package (PMP), to quantitatively  
81 synthesize results from the archive of CMIP simulations via performance metrics that help characterize the overall  
82 agreement between models and observations (Gleckler et al., 2016). In this paper, we describe the latest update of the  
83 PMP and its focus on providing a diverse suite of summary statistics that can be used to construct "quick-look"  
84 summaries of ESM performance from simulations made publicly available to the research community, notably CMIP.  
85 For our purposes, "performance metrics" are typically (but not exclusively) well-established statistical measures that



86 quantify the consistency between observed and simulated characteristics. One goal of the PMP is to further diversify  
87 the suite of high-level performance tests that help characterize the simulated climate. The results provided by the PMP  
88 are frequently used to address two overarching and recurring questions: 1) What are the relative strengths and  
89 weaknesses between different models? and 2) How are models improving with further development? Addressing the  
90 second question is often referred to as “benchmarking” and this motivates an important emphasis of the effort  
91 described in this paper—striving to advance the documentation of all data and results of the PMP in an open and  
92 ultimately reproducible manner.

93 The rest of the paper is organized as follows. In section 2, we provide a technical description of the PMP and  
94 its accompanying reference datasets. In section 3, we describe various sets of simulation metrics that capture an  
95 increasingly comprehensive range of physical processes and time scales ranging from hours to centurial. In section 4,  
96 we introduce the usage of PMP for model benchmarking. In section 5, we discuss the remaining challenges, and we  
97 conclude in section 6 with a summary and future direction.

98

## 99 **2 Software package and data description**

100 The PMP is a Python-based open-source software framework ([https://github.com/PCMDI/pcmdi\\_metrics](https://github.com/PCMDI/pcmdi_metrics)) designed  
101 to objectively gauge the consistency between ESMs and available observations via well-established statistics. The  
102 PMP has been mainly used for the evaluation of CMIP-class models. A subset of CMIP experiments are particularly  
103 well suited to comparing models with observations. The experiments of particular interest include those involving  
104 prescribed sea surface temperature (SST) in accordance with the AMIP protocol, as well as coupled model simulations  
105 labeled as “Historical” that are driven by varying natural and anthropogenic forcings. Some of the metrics applicable  
106 to these experiments may also be relevant to others (e.g., multi-century coupled control runs called “PiControl” and  
107 idealized “4xCO<sub>2</sub>” simulations that are designed for estimating climate sensitivity).

108 The PMP has been applied to multiple generations of CMIP in a quasi-operational fashion as new simulations  
109 are made available, new analysis methods are incorporated, or new observational data become accessible. Shortly  
110 after simulations from the most recent phase of the CMIP (i.e., CMIP6) became accessible, PMP quick-look  
111 summaries were provided on the PCMDI’s website (<https://pcmdi.llnl.gov/metrics/>), offering a resource to scientists  
112 involved in CMIP or others interested in the evaluation of ESMs. To facilitate this, in PCMDI the PMP is technically  
113 linked to the Earth System Grid Federation (ESGF) that is a primary CMIP data delivery infrastructure (Williams et  
114 al., 2016).

115 The PMP is designed to readily work with model output that has been processed using the Climate Model  
116 Output Rewriter (CMOR; <https://cmor.llnl.gov/>), which is a software library developed to prepare model output as  
117 CF-compliant (Hassell et al., 2017; Eaton et al., 2022, <http://cfconventions.org/>) netCDF files. The CMOR is used by  
118 most modeling groups contributing to CMIP, ensuring all model output adheres to the CMIP data structures that  
119 themselves are based on the CF conventions. It is possible to use the PMP on model output that has not been prepared  
120 by CMOR, but this usually requires additional work, e.g., mapping the data to meet the community standards.

121 For reference datasets, the PMP uses observational products processed to be compliant with the Observations  
122 for Model Intercomparison Projects (obs4MIPs; <https://pcmdi.github.io/obs4MIPs/>). The obs4MIPs effort was



123 initiated circa 2010 (Gleckler et al., 2011) to advance the use of the observations in model evaluation and research.  
124 Substantial progress has been made in establishing obs4MIPs data standards that technically align with CMIP model  
125 output (e.g., Teixeira et al., 2014; Ferraro et al., 2015), with the data products published on the ESGF (Waliser et al.,  
126 2020). Obs4MIPs-compliant data were prepared with CMOR, and the data directly available via obs4MIPs are used  
127 as PMP reference datasets.

128 The PMP leverages other Python-based open-source libraries. A primary fundamental tool used in the latest  
129 PMP version is the Python package, Xarray Climate Data Analysis Tools (xCDAT; Vo et al., 2023;  
130 <https://xcdat.readthedocs.io>). The xCDAT is developed to provide a more efficient, robust, and streamlined user  
131 experience in climate data analysis when using xarray (<https://docs.xarray.dev/>). Portions of the PMP rely on the  
132 precursor of the xCDAT, a Python library called Community Data Analysis Tools (CDAT, Williams et al., 2009;  
133 Williams, 2014; Doutriaux et al., 2019), which has been fundamental since the early development stages of the PMP.  
134 The xarray software provides much of the functionality of CDAT (e.g., I/O, indexing, and subsetting). However, it  
135 lacks some key climate domain features that have been frequently used by scientists and exploited by the PMP (e.g.,  
136 regridding, utilization of spatial/temporal bounds for computational operations) which motivated the development of  
137 the xCDAT. Completing the transition from CDAT to xCDAT is a technical priority for the next version of PMP.

138 The primary delivery output of the PMP is the summary statistics. We strive to make the baseline results (raw  
139 statistics) publicly available and well-documented, and continue to make advances with this priority. For our purposes,  
140 we are referring to model performance “summary statistics” and “metrics” interchangeably, although in some  
141 situations we consider there to be an important distinction. For us, a genuine performance metric constitutes a well-  
142 defined and established statistic that has been used in a very specific way (e.g., a particular variable, analysis, and  
143 domain) for long-term benchmarking (see Section 4). The distinction between summary statistics and metrics is  
144 application-dependent and evolving as the community advances efforts to establish quasi-operational capabilities to  
145 gauge ESM performance. Some visualization capabilities described in Section 3 are made available through the PMP.  
146 Users can also further explore the model data comparisons using their preferred visualization methods or incorporate  
147 the results into their own studies from the summary statistics from the PMP. Noting the above, the scope of the PMP  
148 is fairly targeted. It is not intended to be “all-purpose”, e.g. by incorporating the vast range of diagnostics used in  
149 model evaluation.

150 To help advance open and reproducible science, the PMP has been maintained with an open-source policy  
151 with accompanying metadata for data reproducibility and reusability. The PMP code is distributed and released with  
152 version control. Online documentation ([http://pcmdi.github.io/pcmdi\\_metrics/](http://pcmdi.github.io/pcmdi_metrics/)), including user demo Jupyter  
153 Notebooks, and a database of pre-calculated PMP statistics for all AMIP and Historical simulations in the CMIP  
154 archive are also available online. The archive of these statistics stored as JSON files (Crockford, 2006; Crockford and  
155 Morningstar, 2017) includes versioning details for all codes, and dependencies and data that were used for the  
156 calculations. These files provide the baseline results of the PMP (See the Code and Data Availability section for  
157 details). Advancements in model evaluation along with the number of models and complexity of simulations motivate  
158 more systematic documentation of performance summaries. With PMP workflow provenance information being



159 recorded and the model and observational data standards maintained by PCMDI and colleagues, PMP strives to make  
160 all its results reproducible.

161

### 162 **3 Current PMP capabilities**

163 The PMP builds upon model performance tests that have resulted from research at PCMDI and via close  
164 collaborations. Contributors have helped expand the PMP beyond its traditional large-scale performance summaries  
165 of the mean climate (Gleckler et al., 2008). Various evaluation metrics have been implemented to the PMP for climate  
166 variability such as El Niño-Southern Oscillation (ENSO) (Planton et al., 2021; Lee et al., 2021a), extratropical modes  
167 of variability (Lee et al., 2019, 2021b), intra-seasonal oscillation (Ahn et al., 2017), monsoons (Sperber and  
168 Annamalai, 2014), cloud feedback (Zelinka et al., 2022), and the characteristics of simulated precipitation  
169 (Pendergrass et al., 2020; Ahn et al., 2022, 2023) and extremes (Wehner et al., 2020, 2021). This section will provide  
170 an overview of each category of the current PMP evaluation metrics with their usage demonstrations.

171

#### 172 **3.1 Climatology**

173 Mean state metrics quantify how well models simulate observed climatological fields at a large scale, gauged by a  
174 suite of well-established statistics that have been used in climate research for decades. The focus is on the coupled  
175 “Historical” and atmospheric-only AMIP (Gates et al., 1999) simulations which are well-suited for comparison with  
176 observations. The PMP extracts seasonally and annually averaged fields of multiple variables from large-scale  
177 observationally based datasets and results from model simulations. Different obs4MIPs-compliant reference datasets  
178 are used depending on the variable examined. When multiple reference datasets are available, one of them is  
179 considered as a “default” while others are identified as “alternatives”. The default datasets are typically state-of-the-  
180 art products, but in general, we lack definitive measures as to which is the most accurate, so the PMP metrics are  
181 routinely calculated with multiple products so that it can be determined what difference the selection of alternative  
182 observations makes to judgment made about model fidelity. The suite of mean climate metrics (all area weighted)  
183 includes spatial and spatiotemporal root-mean-square error (RMSE), centered spatial RMSE, spatial-mean bias, spatial  
184 standard deviation, spatial pattern correlation, and spatial and spatiotemporal mean absolute error (MAE) of the annual  
185 or seasonal climatological time-mean (Gleckler et al., 2008). Often, a space-time statistic is used that gauges both the  
186 consistency of the observed and simulated climatological pattern as well as its seasonal evolution (see Eq. 1 from  
187 Gleckler et al., 2008). By default, results are available for selected large-scale domains, including: “Global”, “Northern  
188 Hemisphere (NH) Extratropics” (30°N-90°N), “Tropics” (30°S-30°N), and “Southern Hemisphere (SH) Extratropics”  
189 (30°S-90°S). For each domain, results can also be computed for the land and ocean, land only, or ocean only. These  
190 commonly used domains highlight the application of the PMP mean climate statistics at large to global scales, but we  
191 note that PMP allows users to define their own domains of interest, including at regional scales.

192 Although the primary deliverable of the PMP is the metrics, these PMP results can be visualized in various  
193 ways. For individual fields, we often first plot Taylor Diagrams, a polar plot leveraging the relationship between the  
194 centered RMS, the pattern correlation, and the observed and simulated standard deviation (Taylor, 2001). The Taylor  
195 Diagram has become a standard plot in the model evaluation workflow across modeling centers and research



196 communities (see Section 5). To interpret results across CMIP models for many variables, we routinely construct  
197 normalized Portrait Plots or Gleckler Plots (Gleckler et al., 2008) that provide a quick-look examination of the  
198 strengths and weaknesses of different models. For example, in Figure 1, the PMP results display quantitative  
199 information of simulated seasonal climatologies of various meteorological model variables via a normalized global  
200 spatial RMSE (Gleckler et al., 2008). Variants of this plot have been widely used for presenting model evaluation  
201 results, for example, in the Intergovernmental Panel on Climate Change (IPCC) Fifth (Flato et al., 2014, Figures 9.7,  
202 9.12, and 9.37) and Sixth Assessment Reports (Eyring et al., 2021, Chapter 3, Figure 3.42). Because the error  
203 distribution across models is variable dependent, the statistics are often normalized to help reveal differences, in this  
204 case via the median RMSE across all models (see Gleckler et al. 2008 for more details). This normalization enables a  
205 common color scale to be used for all statistics on the Portrait Plot, highlighting the relative strengths and weaknesses  
206 of different models. In this example (Fig. 1), an error of -0.5 indicates that a model's error is 50% smaller than the  
207 typical (median) error across all models, whereas an error of 0.5 is 50% larger than the typical error in the multi-model  
208 ensemble. In many cases, the horizontal bands in the Gleckler plots show that simulations from a given modeling  
209 center have similar error structures relative to the multi-model ensemble.

210 The Parallel Coordinate Plot (Inselberg, 1997, 2008, 2016; Johansson and Forsell, 2016) that retains the  
211 absolute value of the error statistics is used to complement the Portrait plot. Some previous studies have utilized  
212 Parallel Coordinate Plots for analyzing climate model simulations (e.g., Steed et al., 2012; Wong et al., 2014; Wang  
213 et al., 2017), but to date, only a few studies have applied it to collective multi-ESM evaluations (e.g., see Fig. 7 of  
214 Boucher et al., 2020). In the PMP, we generally construct Parallel Coordinate Plots using the same data as in a portrait  
215 plot. However, a fundamental difference is that metrics values can be more easily scaled to highlight absolute values  
216 rather than the normalized relative results of the portrait plot. In this way, the Portrait and Parallel Coordinate plots  
217 complement one another, and in some applications, it can be instructive to display both. Figure 2 shows the  
218 spatiotemporal RMSE, defined as the temporal average of spatial RMSE calculated in each month of the annual cycle,  
219 of CMIP5 and CMIP6 models in the format of Parallel Coordinate Plot. Each vertical axis represents a different scalar  
220 measure gauging a distinct aspect of model fidelity. While polylines are frequently used to connect data points from  
221 the same source (i.e., metric values from the same model, in our case) in Parallel Coordinate Plots, we display results  
222 from each model using an identification symbol to reduce visual clutter on the plot and help identify outlier models.  
223 In the example of Fig. 2, each vertical axis is aligned with the median value midway through its max/min range scale.  
224 Thus, for each axis, the models in the lower half of the plot perform better than the CMIP5-CMIP6 multi-model  
225 median, while in the upper half, the opposite is true. For each vertical axis that is for a different model variable, we  
226 have added violin plots (Hintze and Nelson, 1998) to show probability density functions representing the distributions  
227 of model performance obtained from CMIP5 (shaded in blue, left side of the axis) and CMIP6 (shaded in orange, right  
228 side of the axis). Medians of each CMIP5 and CMIP6 group are highlighted using polylines, which indicates that the  
229 RMSE is reduced in CMIP6 relative to CMIP5 in general for the majority of the subset of model variables.

230



### 231 3.2 *El Niño-Southern Oscillation*

232 The El Niño-Southern Oscillation (ENSO) is Earth's dominant interannual mode of climate variability, which impacts  
233 global climate via both regional oceanic effects and far-reaching atmospheric teleconnections (McPhaden et al., 2006,  
234 2020). In response to increasing interest in a community approach to ENSO evaluation in models (Bellenger et al.,  
235 2014), the International Climate and Ocean Variability, Predictability and Change (CLIVAR) Research Focus on  
236 ENSO in a Changing Climate, together with the CLIVAR Pacific Region Panel, developed the CLIVAR ENSO  
237 Metrics Package (Planton et al., 2021) which is now utilized within the PMP. The ENSO metrics are divided into three  
238 Metrics Collections: *Performance* (i.e., background climatology and basic ENSO characteristics), *Teleconnections*  
239 (ENSO's worldwide teleconnections), and *Processes* (ENSO's internal processes and feedback). Planton et al. (2021)  
240 found that CMIP6 models generally outperform CMIP5 models in several ENSO metrics in particular for those related  
241 to tropical Pacific seasonal cycles and ENSO teleconnections. This effort is discussed in more detail in Planton et al.  
242 (2021), and detailed descriptions of each metric in the package are available in the ENSO Package online open-source  
243 code repository on its GitHub Wiki pages (see [https://github.com/CLIVAR-PRP/ENSO\\_metrics/wiki](https://github.com/CLIVAR-PRP/ENSO_metrics/wiki)).

244 Figure 3 demonstrates the application of the ENSO metrics to CMIP6, showing the magnitudes of inter-  
245 model and inter-ensemble spreads, along with observational uncertainty varying across metrics. For a majority of the  
246 ENSO Performance metrics model error and inter-model spread are substantially larger than observational uncertainty  
247 (Figs. 3a-n). This highlights the systematic biases like the double ITCZ (Fig. 3a) that are persisting through CMIP  
248 phases (Tian and Dong, 2020). Similarly, ENSO Processes metrics (Figs. 3t-w) indicate large errors in the feedback  
249 loops generating SST anomalies, indicating a different balance of processes in the model and in the reference and  
250 possibly compensating errors (Bayr et al., 2019, Guilyardi et al. 2020). In contrast, for ENSO Teleconnection metrics,  
251 the observational uncertainty is substantially larger, thus challenging validation of model error (Figs. 3o-r). For some  
252 metrics, such as the ENSO duration (Fig. 3f), the ENSO Asymmetry metric (Fig. 3i), and the Ocean driven SST metric  
253 (Fig. 3s), there are larger inter-ensemble spreads than the inter-model spreads. From such results, Lee et al. (2021a)  
254 examined the inter-model and inter-member spread of these metrics from the large ensembles available from CMIP6  
255 and the US CLIVAR Large Ensemble Working Group. They argued that to robustly characterize baseline ENSO  
256 characteristics and physical processes, larger ensemble sizes are needed, compared to existing state-of-the-art  
257 ensemble projects.

258

### 259 3.3 *Extratropical Modes of Variability*

260 The PMP includes objective measures of the pattern and amplitude of extratropical modes of variability from  
261 PCMDI's research, which has expanded beyond its traditional large-scale performance summaries to include  
262 interannual variability, considering increasing interest in setting an objective approach for the collective evaluation of  
263 multiple modes. Extratropical modes of variability (ETMoV) metrics in the PMP were developed by Lee et al. (2019a)  
264 that stem from earlier works (e.g., Stoner et al., 2009; Phillips et al., 2014). Lee et al. (2019a) illustrated a challenge  
265 when evaluating modes of variability using the traditional empirical orthogonal functions (EOF). In particular, when  
266 a higher-order EOF of a model more closely corresponds to a lower-order observationally based EOF (or vice versa),  
267 it can significantly affect conclusions drawn about model performance. To circumvent this issue in evaluating the





268 interannual variability modes, Lee et al. (2019a) used the Common Basis Function (CBF) approach that projects the  
269 observed EOF pattern onto model anomalies. This approach has been previously applied for the evaluation of  
270 intraseasonal variability modes (Sperber, 2004; Sperber et al., 2005), and recently for Antarctic climate change (Jun  
271 et al., 2020), seasonal-to-decadal predictability associated with the ENSO (Choi and Son, 2022). In the PMP, the CBF  
272 approach is taken as a default method, and the traditional EOF approach is also enabled as an option for the ETMoV  
273 metrics calculations.

274 The ETMoV metrics in the PMP measure simulated patterns and amplitudes of ETMoV, and quantify their  
275 agreement with observations (e.g., Lee et al., 2019a, 2021b). The PMP's ETMoV metrics evaluate 5 atmospheric  
276 modes – the Northern Annular Mode (NAM), North Atlantic Oscillation (NAO), Pacific North America pattern  
277 (PNA), North Pacific Oscillation (NPO), and Southern Annular Mode (SAM), and 3 ocean modes diagnosed by the  
278 variance of sea-surface temperature – Pacific Decadal Oscillation (PDO), North Pacific Gyre Oscillation (NPGO),  
279 and Atlantic Multi-decadal Oscillation (AMO). The AMO is included for experimental purposes, considering the  
280 significant uncertainty in detecting the AMO (Deser and Philips 2021; Zhao et al., 2022). The amplitude metric,  
281 defined as the ratio of standard deviations of the model and observed principal components, has been used to examine  
282 the evolution of the performance of models across different CMIP generations (Fig. 4, adapted from Lee et al., 2021b).  
283 Green shading predominates, indicating where the simulated amplitude of variability is similar to observations. In  
284 some cases, such as for SAM\_SON, the models overestimate the observed amplitude. Other authors have used Portrait  
285 plots to synthesize CMIP performance of simulated variability (e.g., Sillmann et al., 2013; Bellenger et al., 2014;  
286 Cannon 2020; Kim et al., 2020; Planton et al., 2020; Zhang et al., 2021; Ahn et al., 2022, 2023).

287 The PMP's ETMoV metrics have been used in several model evaluation studies. For example, Orbe et al.  
288 (2020) analyzed models from U.S. climate modeling groups including DOE, National Aeronautics and Space  
289 Administration (NASA), National Center for Atmospheric Research (NCAR), and National Oceanic and Atmospheric  
290 Administration (NOAA), where they found that the improvement in the ETMoV performance is highly dependent on  
291 mode and season, when comparing across different generations of those models. Sung et al. (2021) examined the  
292 performance of models run at the Korea Meteorological Administration (K-ACE and UKESM1) in reproducing  
293 ETMoVs from their Historical simulations, and concluded that these models reasonably capture most ETMoVs. Lee  
294 et al. (2021b) collectively evaluated ~130 models from CMIP3, 5, and 6 archive databases using their ~850 Historical  
295 and ~300 AMIP simulations, where they found the spatial pattern skill improved in CMIP6 compared to CMIP5 or  
296 CMIP3 for most modes and seasons, while the improvement in amplitude skill is not clear. Arcodia et al. (2023) used  
297 the PMP to derive PDO and AMO to investigate their role in decadal variability of subseasonal predictability of  
298 precipitation over the western coast of North America and concluded that no significant relationship was found.

299

### 300 **3.4 Intraseasonal Oscillation**

301 The PMP has implemented metrics for the Madden-Julian Oscillation (MJO; Madden and Julian, 1971, 1972, 1994).  
302 The MJO is the dominant mode of tropical intraseasonal variability, characterized by a pronounced eastward  
303 propagation of large-scale atmospheric circulation coupled with convection with a typical periodicity of 30-60 days.



304 Selected metrics from the MJO diagnostics package, developed by the CLIVAR MJO Working Group (Waliser et al.,  
305 2009), have been implemented in the PMP following Ahn et al. (2017).

306 We particularly focused on a metric called East/West power Ratio (hereafter, EWR) and East power  
307 normalized by Observation (hereafter, EOR). The EWR, proposed by Zhang and Hendon (1997), is defined as the  
308 ratio of the total spectral power over the MJO band (eastward propagating, wavenumber 1-3 and period of 30-60 days)  
309 to that of its westward propagating counterpart in the wavenumber-frequency power spectra. The EWR metric has  
310 been widely used in the community, to examine the robustness of the eastward propagating feature of the MJO (e.g.,  
311 Zhang and Hendon, 1997; Hendon et al., 1999; Lin et al., 2006; Kim et al., 2009; Ahn et al., 2017). The EOR is  
312 formulated by normalizing a model's spectral power within the MJO band by the corresponding observed value. Ahn  
313 et al. (2017) showed EWRs and EORs of the CMIP5 models. Using daily precipitation, the PMP calculates EWR and  
314 EOR separately for boreal winter (November to April) and boreal summer (March to October). We apply the  
315 frequency-wavenumber decomposition method to precipitation from observations (GPCP-based; 1997-2010) and the  
316 CMIP5 and CMIP6 Historical simulations for 1985-2004. For disturbances with wavenumbers 1-3 and frequencies  
317 corresponding to 30-60 days, it is clear in observations that the eastward propagating signal dominates over its  
318 westward propagating counterpart with an EWR value of about 2.49 (Fig. 5a). Figure 5b shows the wavenumber-  
319 frequency power spectrum from CMIP5 IPSL-CM5B-LR as an example, which has an EWR value that is comparable  
320 to the observed value.

321 Figure 6 shows the EWR from individual models' multiple ensemble members and their average. The average  
322 EWR of the CMIP6 model simulations is more realistic than that of the CMIP5 models. Interestingly, a substantial  
323 spread exists across models and also among ensemble members of a single model. For example, while the average  
324 EWR value for the CESM2 ensemble is 2.47 (close to 2.49 from GPCP observations), the EWR values of the  
325 individual ensemble members range from 1.87 to 3.23. Kang et al. (2020) suggested that the ensemble spread in the  
326 propagation characteristics of the MJO can be attributed to the differences in the moisture mean state, especially its  
327 meridional moisture gradient. A cautionary note should be given to the fact that the MJO frequency and wavenumber  
328 windows are chosen to capture the spectral peak in observations. Thus, while the EWR provides an initial evaluation  
329 of the propagation characteristics of the observed and simulated MJO, it is instructive to look at the frequency-  
330 wavenumber spectra, as in some cases the dominant periodicity and wavenumber in a model may be different than in  
331 observations. It is worthwhile to note that the PMP can be used to obtain EWR and EOR of other daily variables for  
332 MJO analysis, such as outgoing longwave radiation (OLR) or zonal wind at 850 hPa (U-850) or 250 hPa (U-250), as  
333 shown in Ahn et al. (2017).

334

### 335 **3.5 Monsoons**

336 Based on the work of Sperber and Annamalai (2014), skill metrics in the PMP quantify how well models represent  
337 the onset, decay, and duration of regional monsoons. From observations and Historical simulations, the climatological  
338 pentads of precipitation are area-averaged for six monsoon-related domains: All-India Rainfall, Sahel, Gulf of Guinea,  
339 North American Monsoon, South American Monsoon, and Northern Australia, as seen in Fig. 7. For the domains in  
340 the Northern Hemisphere, the 73 climatological pentads run from January to December, while for the domains in the



341 Southern Hemisphere, the pentads run from July to June. For each domain, the precipitation is accumulated at each  
342 subsequent pentad and then divided by the total precipitation to give the fractional accumulation of precipitation as a  
343 function of pentad. Thus, the annual cycle behavior is evaluated irrespective of whether a model has a dry or wet bias.  
344 Except for GoG, the onset and decay of monsoon occur for a fractional accumulation of 0.2 and 0.8, respectively.  
345 Between these fractional accumulations, the accumulation of precipitation is nearly linear as the monsoon season  
346 progresses. Comparison of the simulated and observed onset, duration, and decay are presented in terms of the  
347 difference in the pentad index obtained from the model and observations (i.e., model minus observations). Therefore,  
348 negative values indicate that the onset or decay in the model occurs earlier than in observations, while positive values  
349 indicate the opposite. For duration, negative values indicate that for the model it takes fewer pentads to progress from  
350 onset to decay compared to observations (i.e., the simulated monsoon period is too short), while positive values  
351 indicate the opposite.

352 For CMIP5, we find systematic errors in the phase of the annual cycle of rainfall. The models are delayed in  
353 the onset of summer rainfall over India, the Gulf of Guinea, and the South American Monsoon, with early onset  
354 prevalent for the Sahel and the North American Monsoon. The lack of consistency in the phase error across all domains  
355 suggests that a “global” approach to the study of monsoons may not be sufficient to rectify the regional differences.  
356 Rather, regional process studies are necessary for diagnosing the underlying causes of the regionally specific  
357 systematic model biases over the different monsoon domains. Assessment of the monsoon fidelity in CMIP6 models  
358 using the PMP is in progress.

359

### 360 **3.6 Cloud feedback and mean-state**

361 Uncertainties in cloud feedback are the primary driver of model-to-model differences in climate sensitivity – the global  
362 temperature response to a doubling of atmospheric CO<sub>2</sub>. Recently, an expert synthesis of several lines of evidence  
363 spanning theory, high-resolution models, and observations was conducted to establish quantitative benchmark values  
364 (and uncertainty ranges) for several key cloud feedback mechanisms. The assessed feedbacks are those due to changes  
365 in high-cloud altitude, tropical marine low-cloud amount, tropical anvil cloud area, land cloud amount, middle latitude  
366 marine low-cloud amount, and high latitude low-cloud optical depth. The sum of these six components yields the total  
367 assessed cloud feedback, which is part of the overall radiative feedback that fed into the Bayesian calculation of  
368 climate sensitivity in Sherwood et al. (2020). Zelinka et al. (2022) estimated these same feedback components in  
369 climate models and evaluated them against the expert-judgment values determined in Sherwood et al. (2020),  
370 ultimately deriving a root mean square error metric that quantifies the overall match between each model’s cloud  
371 feedback and those determined through expert judgment.

372 Figure 8 shows the model-simulated values for each individual feedback computed in *amip-p4K* simulations  
373 as part of CMIP5 and CMIP6 alongside the expert judgment values. Each model is color-coded by its equilibrium  
374 climate sensitivity (determined using *abrupt-4CO2* simulations as described in Zelinka et al., 2020), and the values  
375 from an illustrative model (GFDL-CM4) are highlighted. Among the key results apparent from this figure is that  
376 models typically underestimate the strength of both positive tropical marine low-cloud feedback and the negative anvil  
377 cloud feedback relative to the central expert assessed value. The sum of all six assessed feedback components is



378 positive in all but two models, with a multimodel mean value that is close to the expert-assessed value, but exhibits  
379 substantial intermodel spread.

380 In addition to evaluating the ability of models to match the assessed cloud feedback components, Zelinka et  
381 al. (2022) investigated whether models with less erroneous mean-state clouds tend to have smaller errors in their  
382 overall cloud feedback RMSE. This involved computing the mean-state cloud property error metric developed by  
383 Klein et al. (2013). This error metric quantifies the spatiotemporal error in climatological cloud properties for clouds  
384 with optical depths greater than 3.6, weighted by their net TOA radiative impact. The observational baseline against  
385 which the models are compared comes from the ISCCP HGG dataset (Young et al., 2018). Zelinka et al. (2022)  
386 showed that models with smaller mean-state cloud errors tend to have stronger but not necessarily better (less  
387 erroneous) cloud feedback, which suggests that improving mean-state cloud properties does not guarantee  
388 improvement in the cloud response to warming. However, the models with the smallest errors in cloud feedback tend  
389 to also have less erroneous mean-state cloud properties, and no models with poor mean-state cloud properties have  
390 feedback in good agreement with expert judgment.

391 The PMP implementation of this code computes cloud feedback by differencing fields from *amip-p4K* and  
392 *amip* experiments and normalizing by the corresponding global mean surface temperature change rather than from  
393 differencing *abrupt-4xCO2* and *piControl* experiments and computing feedback via regression (as was done in Zelinka  
394 et al., 2022). This choice is made to reduce the computational burden and also because cloud feedbacks derived from  
395 these simpler atmosphere-only simulations have been shown to closely match those derived from fully coupled  
396 quadrupled CO<sub>2</sub> simulations (Qin et al., 2022). The code produces figures in which the user-specified model results  
397 are highlighted and placed in the context of the CMIP5 and CMIP6 multi-model results (e.g., Figure 8).

398

### 399 **3.7 Precipitation**

400 Recognizing the importance of accurately simulating precipitation in ESMs and a lack of objective and systematic  
401 benchmarking for it, and motivated by discussions with WGNE and WGCM working groups of WCRP, the DOE has  
402 initiated an effort to establish a pathway to help modelers gauge improvement (U.S. DOE, 2020). The 2019 DOE  
403 workshop “Benchmarking Simulated Precipitation in Earth System Models” generated two sets of precipitation  
404 metrics: *baseline* and *exploratory* metrics (Pendergrass et al., 2020). In the PMP, we have focused on implementing  
405 the *baseline* metrics for benchmarking simulated precipitation. In parallel, a set of *exploratory* metrics that could be  
406 added to metrics suites including PMP in the future was illustrated by Leung et al. (2022) to extend the evaluation  
407 scope to include process-oriented and phenomena-based diagnostics and metrics.

408 The *baseline* metrics gauge the consistency between ESMs and observations, focusing on the holistic set of  
409 observed rainfall characteristics (Fig. 9). For example, the spatial distribution of mean state precipitation and seasonal  
410 cycle are outcomes of the PMP’s Climatology metrics (described in Section 3.1), which provides collective evaluation  
411 statistics such as RMSE, standard deviation, and pattern correlation over various domains (e.g., global, NH and SH  
412 extratropics, and Tropics, with each domain as a whole, and over land and ocean, in separate). Evaluation of  
413 precipitation variability across many timescales with PMP is documented in Ahn et al. (2022); we summarize some  
414 of the findings here. The precipitation variability metric measures forced (diurnal and annual cycles) and internal



415 variability across timescales (subdaily, synoptic, subseasonal, seasonal, and interannual) in a framework based on  
416 power spectra of 3-hourly total and anomaly precipitation. Overall, CMIP5 and CMIP6 models underestimate the  
417 internal variability, which is more pronounced in the higher frequency variability, while they overestimate the forced  
418 variability (Fig. 10). For the diurnal cycle, PMP includes metrics from Covey et al. (2016). Additionally, the intensity  
419 and distribution of precipitation are assessed following Ahn et al. (2023). Extreme daily precipitation indices and their  
420 20-year return values are calculated using a non-stationary Generalized Extreme Value statistical method. From the  
421 CMIP5 and CMIP6 historical simulations we evaluate model performance of these indices and their return values in  
422 comparison with gridded land-based daily observations. Using this approach, Wehner et al. (2020) found that at  
423 models' standard resolutions, no meaningful differences were found between the two generations of CMIP models.  
424 Wehner et al. (2021) extended the evaluations of simulated extreme precipitation to seasonal 3-hourly precipitation  
425 extremes produced by available HighResMIP models and concluded that the improvement is minimal with the models'  
426 increased spatial resolutions. They also noted that the order of operations of regridding and calculating extremes  
427 affects the ability of models to reproduce observations. Drought metrics developed by Xue and Ullrich (2021) are not  
428 implemented in PMP directly, but are wrapped by the Coordinated Model Evaluation Capabilities (CMEC; Ordonez  
429 et al. 2021), which is a parallel framework for supporting community-developed evaluation packages. Together, these  
430 metrics provide a streamlined workflow for running the entire baseline metrics via the PMP and CMEC that is ready  
431 for use by operational centers and in the CMIP7.

432

### 433 *3.8 Relating metrics to underlying diagnostics*

434 Considering the extensive collection of information generated from the PMP, efforts have supported improved  
435 visualizations of metrics using interactive graphic user interfaces. These capabilities can facilitate the interpretation  
436 and synthesis of vast amounts of information associated with the diverse metrics and the underlying diagnostics from  
437 which they were derived. Via the interactive navigation interface, we can explore the underlying diagnostics behind  
438 the PMP's summary plots. On the PCMDI website, we provide interactive graphical interfaces to enable navigating  
439 the supporting plots to the underlying diagnostics of each model's ensemble members and their average. For example,  
440 on the interactive mean climate plots ([https://pcmdi.llnl.gov/metrics/mean\\_clim/](https://pcmdi.llnl.gov/metrics/mean_clim/)), hovering the mouse cursor over a  
441 square or triangle in the Portrait Plot, or over the markers or lines in the Parallel Coordinate Plot, reveals the diagnostic  
442 plot from which the metrics were generated. It allows the user to toggle between several metrics (e.g., RMSE, bias,  
443 and correlation) and regions (e.g., global, Northern/Southern Hemisphere, and Tropics), along with relevant  
444 provenance information. Users can click on the interactive plots to get dive-down diagnostics information for the  
445 model of interest which provides detailed analysis to better understand how the metric was calculated. As with the  
446 PMP's mean climate metrics output, we currently provide interactive summary graphics for ENSO  
447 (<https://pcmdi.llnl.gov/metrics/enso/>), extratropical modes of variability  
448 ([https://pcmdi.llnl.gov/metrics/variability\\_modes/](https://pcmdi.llnl.gov/metrics/variability_modes/)), monsoon (<https://pcmdi.llnl.gov/metrics/monsoon/>), MJO  
449 (<https://pcmdi.llnl.gov/metrics/mjo/>), and precipitation benchmarking (<https://pcmdi.llnl.gov/metrics/precip/>). We  
450 plan to expand this capability to other metrics in the PMP, such as the cloud feedback analysis. The majority of the



451 PMP's interactive plots have been developed using Bokeh (<https://bokeh.org/>), a Python data visualization library that  
452 enables the creation of interactive plots and applications for web browsers.

453

#### 454 **4 Model Benchmarking**

455 While the PMP originally focused on evaluating multiple models (e.g., Gleckler et al., 2008), in parallel there has  
456 been increasing interest from model developers and modeling centers to leverage the PMP to track performance  
457 evolution in the model development cycle, as discussed in Gleckler et al. (2016). For example, metrics from the PMP  
458 have been used to document performance of ESMs developed in the U.S. DOE Exascale Earth System Model (E3SM;  
459 Caldwell et al., 2019; Golaz et al., 2019; Rasch et al., 2019; Hannah et al., 2021; Tang et al., 2021), NOAA  
460 Geophysical Fluid Dynamics Laboratory (GFDL; Zhao et al., 2018), Institut Pierre-Simon Laplace (IPSL; Boucher et  
461 al., 2020; Planton et al., 2021), National Institute of Meteorological Sciences-Korea Meteorological Administration  
462 (NIMS-KMA; Sung et al., 2021), University of California, Los Angeles (Lee et al., 2019b), and the Community  
463 Integrated Earth System Model (CIESM) project (Lin et al., 2020).

464 To make the PMP more accessible and useful for modeling groups, efforts are underway to broaden workflow  
465 options. Currently, a typical application involves computing a particular class of performance metrics (e.g., mean  
466 climate) for all CMIP simulations available via ESGF. To facilitate the ability of modeling groups to routinely use the  
467 PMP during their development process, we are working to provide a customized workflow option to run all the PMP  
468 metrics more seamlessly on a single model, and to compare these results with a database of PMP results obtained from  
469 CMIP simulations (see Code and Data Availability section). Via the PMP-documented and pre-calculated metrics  
470 from simulations in the CMIP archive, it is possible to readily incorporate CMIP results into the assessment of new  
471 simulations, without retrieving all CMIP simulations and recomputing the results. The resulting quick-look feedback  
472 can highlight model improvement (or deterioration) and can assist in determining development priorities or in the  
473 selection of a new model version.

474 As an example, here, we show PMP results obtained from GFDL-CM3 from CMIP5 and GFDL-CM4 from  
475 CMIP6, for a demonstration of using the Taylor Diagram to compare versions of a given model (Fig. 11). One  
476 advantage of the Taylor Diagram is that it collectively represents three statistics (i.e., centered RMSE, standard  
477 deviation, and correlation) in a single plot (Taylor, 2001), which synthesizes the performance intercomparison of  
478 multiple models (or different versions of a model). In this example, four variables were selected to summarize  
479 performance evolution (shown by arrows) in multiple seasons. Except for boreal winter, both model versions are  
480 nearly identical in terms of net TOA radiation, however in all seasons the longwave cloud radiative effect is clearly  
481 improved in the newer model version. The TOA flux improvements likely contributed to the precipitation  
482 improvements, by improving the balances of radiative cooling and latent heating. The improvement in the newer  
483 model version is consistent with that documented by Held et al., (2019) and evident via the arrow directions pointing  
484 to the observational reference point.

485 Parallel Coordinate Plots can also be used to summarize the comparison of two simulations for their  
486 performance. In this section, as an example we demonstrate the comparison of selected metrics: the mean climate,  
487 ENSO, and ETMoV (Fig. 12). To facilitate comparison of a subset of models, a few models can be selected and



488 highlighted as connected lines across individual vertical axes on the plot. With the PMP, a common application is to  
489 select two versions of the same model to contrast their performance (solid lines) against the backdrop of results from  
490 other models, shown as violin plots for the distribution of statistics from other models on each vertical axis. The  
491 spatiotemporal RMSE (i.e., temporally averaged spatial RMSE of annual cycle climatology patterns) is used for mean  
492 climate as discussed in Section 3.1. The PMP's ENSO metrics that were discussed in Section 3.2 and the RMSE  
493 representing total error of ETMoV that were discussed in Section 3.3 are respectively used for ENSO and ETMoV.  
494 The plot is simplified from Figure 2 to more efficiently highlight the difference in performance of two GFDL models:  
495 GFDL-CM3 and GFDL-CM4. Each vertical axis indicates performance for each metric defined for climatology of  
496 variables (Fig. 12a), ENSO characteristics (Fig. 12b), or interannual variability mode obtained from seasonal or  
497 monthly averaged time series (Fig. 12c). In this example, it is shown that GFDL-CM4 is superior to GFDL-CM3 for  
498 most cases across selected metrics (downward arrows in green) while inferior for a few cases (upward arrows in red)  
499 — consistent with previous findings (Held et al., 2019; Planton et al., 2021; Chen et al., 2021). Such applications of  
500 the Parallel Coordinate Plot can enable quick overall assessment and tracking of the ESM performance evolution  
501 during its development cycle. More examples showing other models are available in the Supplementary material (Figs.  
502 S1 to S3).

503 Note that there have been efforts to coalesce objective model evaluation concepts used in the research  
504 community (e.g., Knutti et al., 2010), however as the field continues to evolve rapidly, definitions are still being  
505 finessed, and there is room for the community to further advance well-established metrics. Via the PMP, we produce  
506 hundreds of summary statistics, but it will not be surprising if only a subset of them might be considered as viable  
507 candidate metrics for more practical routine performance evaluations.

508

## 509 **5 Discussion**

510 Given the critical role ESMs play in our efforts to understand a changing climate, scientists involved in the analysis  
511 of ESM simulations have been compelled to improve the process of model evaluation. Current progress towards  
512 systematic model evaluation remains dynamic, with evolving approaches and many independent paths being pursued.  
513 This has resulted in the development of diversified model evaluation software packages. For example, ESMValTool  
514 (Eyring et al., 2016, 2019, 2020; Righi et al., 2020) is a comprehensive package led by a European core development  
515 team that has been used for numerous applications including producing model evaluation plots in Chapter 3 of the  
516 IPCC's AR6 Working Group 1 Assessment (Eyring et al., 2021). The Model Diagnostics Task Force (MDTF)  
517 Diagnostics package, led by NOAA, focuses on process-oriented diagnostics (Maloney et al., 2019; Neelin et al.,  
518 2023). The International Land Model Benchmarking (ILAMB) Software System (Collier et al., 2018) led by Oak  
519 Ridge National Laboratory provides land surface and carbon cycle metrics with key state-of-the-art observational  
520 products, and similarly, the International Ocean Model Benchmarking (IOMB) Software System (Fu et al., 2022)  
521 focuses on surface and upper ocean biogeochemical variables. The Climate Variability Diagnostics Package (CVDP;  
522 Phillips et al., 2014; Fasullo et al., 2020) developed at NCAR provides diagnosis of climate modes of variability.  
523 Analyzing Scales of Precipitation (ASoP; Klingaman et al., 2017; Martin et al., 2017; Ordonez et al., 2021) focuses  
524 on analyzing precipitation scales across space and time. In parallel, the regional climate community also has actively



525 developed metrics packages such as the Regional Climate Model Evaluation System (RCMES; Lee et al., 2018a;  
526 Whitehall et al. 2012). Separately, a few climate modeling centers have developed their own model evaluation  
527 packages to assist in their in-house ESM development, e.g., the E3SM Diags (Zhang et al., 2022). There also have  
528 been other efforts to enhance the usability of in-situ and field campaign observations in ESM evaluations, such as  
529 Atmospheric Radiation Measurement (ARM) GCM Diag (Zhang et al., 2018, 2020) and Earth System Model Aerosol–  
530 Cloud Diagnostics (ESMAC Diags; Tang et al., 2022, 2023).

531 The model evaluation packages currently being advanced within the ESM research community all have their  
532 own technical approaches and scientific priorities. We believe that this diversity has made, and will continue to make,  
533 the model evaluation process even more comprehensive and successful. The fact that there is some overlap in a few  
534 cases is advantageous because it enables the cross-verification of results, which is particularly useful in the more  
535 complex analyses. Despite the advantages, having no single best or widely accepted approach for the community to  
536 follow, does introduce complexity to the coordination of model evaluation. To facilitate collective usages of individual  
537 evaluation tools, the CMEC has initiated the development of a unified code base that technically coordinates the  
538 operation of distinct but complementary tools (Ordonez et al. 2021). Currently, the PMP, ILAMB, MDTF and ASoP  
539 have become CMEC-compliant by adopting the common interface standards that define how evaluation tools interact  
540 with observational data and climate model output. We expect that CMEC can also help the model evaluation  
541 community to establish standards for archiving the metrics output, much as the community did for the conventions to  
542 describe climate model data (e.g., CMIP application of CF Metadata Conventions [<http://cfconventions.org/>]; Hassell  
543 et al., 2017; Eaton et al., 2022).

544 It is worth noting that the comprehensive database of PMP results offers a resource for exploring the range  
545 of structural errors in CMIP class models and their interrelationships. For example, examination of cross-metric  
546 relationships between mean-state and variability biases can shed additional light on the propagation of errors (e.g.,  
547 Kang et al., 2020; Lee et al., 2021b). There continues to be interest in ranking models for specific applications (e.g.,  
548 Ashfaq et al., 2022; Goldenson et al., 2023; Longmate et al., 2023; Papalexou et al., 2020) or to “move beyond one  
549 model one vote” in multi-model analysis to reduce uncertainties in the spread of multi-model projections (e.g., Knutti,  
550 2010; Knutti et al., 2017; Sanderson et al., 2017; Herger et al., 2018; Hausfather et al., 2022; Merrifield et al., 2023).  
551 While we acknowledge potential interests in using the results of the PMP or equivalent to rank models or identify  
552 performance outliers (e.g., Sanderson and Wehner, 2017), we believe the many challenges associated with model  
553 weighting are application dependent, and thus leave it up to users of the PMP to make those judgments.

554

## 555 **6 Summary and Future Directions**

556 The PMP has provided quasi-operational ESM evaluation capabilities that can be rapidly deployed to objectively  
557 summarize a diverse suite of model behavior with results made publically available. This can be of value in the  
558 assessment of community intercomparisons like CMIP, the evaluation of large ensembles, or the model development  
559 process. By documenting objective performance summaries produced by the PMP and making them available via  
560 detailed version control, additional research is made possible beyond the baseline model evaluation, model  
561 intercomparison, and benchmarking. The outcomes of PMP's calculations applied to the CMIP archive culminate in





562 the PCMDI Simulation Summary (<https://pcmdi.llnl.gov/metrics/>). This summary serves as a comprehensive  
563 repository of PMP outputs, visually capturing the outcomes of objective model-to-observation comparisons. Special  
564 attention is dedicated to the most recent ensemble of models contributing to CMIP6. By offering a comprehensive  
565 assessment of simulated climate, its variability modes, and characteristics of precipitation in ESMs, the PMP  
566 framework equips model developers with quantifiable benchmarks to validate and enhance model performance.

567 With the growing interest in augmenting the suite of metrics within PMP that reflects an evolving landscape  
568 of evaluation needs, continual efforts are channeled into expanding the scope of the PMP. For example, in coordination  
569 with the World Meteorological Organization (WMO)'s WGENE MJO Task Force, additional candidate MJO metrics  
570 for PMP inclusion have been identified to facilitate more comprehensive assessments of the MJO. Implementation of  
571 metrics for MJO amplitude, periodicity, and structure into the PMP is planned. The ongoing collaboration with NCAR  
572 aims to incorporate metrics related to the upper atmosphere, specifically the Quasi-Biennial Oscillation (QBO) and  
573 QBO-MJO metrics (e.g. Kim et al., 2020). We also have plans to grow the scope of PMP beyond its traditional  
574 atmospheric realm to include domains like the ocean and Arctic regions through collaboration with the U.S. DOE's  
575 project entitled High Latitude Application and Testing of ESMs (HiLAT, <https://www.hilat.org/>). This dimension of  
576 evaluation holds promise in offering deeper insights into model performance.

577 In addition to the scientific challenges associated with diversifying objective summaries of model  
578 performance, there are numerous potential areas to advance accompanying technologies, in large part related to the  
579 rapidly evolving set of open-source tools and methods available to scientists. We expect that the current ongoing PMP  
580 code modernization effort to fully adapt the xCDAT will potentially galvanize greater community involvement. We  
581 will continue to maintain robust rigorously in the calculation of statistics for the PMP metrics by staying tuned with  
582 the latest progress in the field, such as implementing the method for more rigorous conservation in horizontal  
583 interpolation (Taylor, 2023). To improve clarity of key deliverable messages from multivariate data of PMP's metrics  
584 obtained from comprehensive ESM archives, we will consider implementing the advances in the high-dimensional  
585 data visualization field, such as the circular plot discussed in Lee et al. (2018b) and variations of Parallel Coordinate  
586 Plots proposed by Hassan et al. (2019) and Lu et al. (2020).

587 Looking ahead, the PMP framework is also poised to contribute to high-resolution climate modeling  
588 communities, notably the High Resolution Model Intercomparison Project (HighResMIP; Haarsma et al., 2016) and  
589 the DYnamics of the Atmospheric general circulation Modeled On Non-hydrostatic Domains (DYAMOND; Stevens  
590 et al., 2019). This motivates developments of specialized metrics for high-resolution models, which demonstrate the  
591 features that high-resolution models have enabled. Potential avenue of exploration involves leveraging Machine  
592 Learning (ML) techniques, considering the examined applicability of ML and other state-of-the-art data science  
593 techniques being used for process-oriented ESM evaluation works (e.g., Nowack et al., 2020; Labe and Barnes, 2022;  
594 Dalelane et al., 2023). Applications of ML detections, such as for storms using TempestExtremes (Ullrich and  
595 Zarzycki 2017; Ullrich et al., 2021) and fronts (e.g. Biard and Kunkel, 2019), can enable additional specialized storm  
596 metrics for high resolution simulations. For convection permitting models, yet more storm metrics can be applied such  
597 as Mesoscale convective systems. Into the PMP, we currently have plans to implement atmospheric blocking metrics  
598 that were developed through the collaboration of Colorado State University and the PCMDI (Valkonen et al., in prep),



599 and Atmospheric River detection metrics that are currently under development at LLNL. Both of these metrics suites  
600 were developed using the pattern detection capabilities in the latest TempestExtremes (Ullrich et al., 2021). This  
601 application of the PMP aligns with a broader plan for regional expansion, with a deliberate emphasis on processes  
602 intrinsic to specific regions.

603 We anticipate that the PMP will continue to play a crucial role in benchmarking ESMs in the future.  
604 Improvements in PMP, coupled with advancements in projects within the MIP community, will significantly  
605 contribute to assessing the evolving performance of ESMs including via the collaboration with the CMIP  
606 Benchmarking Task Team. Enhancements in version control and transparency within obs4MIPs are poised to enhance  
607 the provenance and reproducibility of PMP results, thereby strengthening the foundation for rigorous and repeatable  
608 performance benchmarking. The PMP's collaboration with the CMIP Forcing Task Team, through the Input4MIPs  
609 (Durack et al., 2018) and the CMIP6Plus projects, will further expand the utility of performance metrics in identifying  
610 problems associated with the forcing dataset and their application and use in reproducing the observed record of  
611 historical climate. Furthermore, as ESMs advance towards more operationalized configurations to meet the demands  
612 of decision-making processes (Jakob et al., 2023), the PMP holds significant potential to provide interoperable ESM  
613 evaluation and benchmarking capabilities to the community.

614

#### 615 **Author Contributions**

616 All authors contributed to the design and implementation of the research, analysis of the results, and to writing of the  
617 manuscript. All authors contributed to the development of codes/metrics in the PMP, its ecosystem tools, and/or the  
618 establishment of use cases. JL and PJG led and coordinated the paper with input from all authors.

619

#### 620 **Code and Data Availability**

621 The source code of PMP (Lee et al., 2023b) is available as an open-source Python package:  
622 [https://github.com/PCMDI/pcmdi\\_metrics](https://github.com/PCMDI/pcmdi_metrics) (last access: 21 November 2023) with versions archived on Zenodo DOI:  
623 <https://doi.org/10.5281/zenodo.592790> (last access: 21 November 2023). The PMP results database (Lee et al., 2023a)  
624 that includes calculated metrics is available on the GitHub repository at  
625 [https://github.com/PCMDI/pcmdi\\_metrics\\_results\\_archive](https://github.com/PCMDI/pcmdi_metrics_results_archive) (last access: 21 November 2023) with versions archived  
626 on Zenodo DOI: <https://doi.org/10.5281/zenodo.10181201>. The interactive visualizations of the PMP results are  
627 available on the PCMDI website at <https://pcmdi.llnl.gov/metrics> (last access: 21 November 2023). The CMIP5 and  
628 CMIP6 model outputs and obs4MIPs datasets used in this paper are available via the Earth System Grid Federation at  
629 <https://esgf-node.llnl.gov/> (last access: 21 November 2023).

630

#### 631 **Competing interests**

632 At least one of the (co-)authors is a member of the editorial board of *Geoscientific Model Development*.

633

634



635 **Acknowledgment**

636 We acknowledge the World Climate Research Programme, which, through its Working Group on Coupled Modeling,  
637 coordinated and promoted CMIP6. We thank the climate modeling groups for producing and making available their  
638 model output, the Earth System Grid Federation (ESGF) for archiving the data and providing access, and the multiple  
639 funding agencies that support CMIP6 and ESGF. This work is performed under the auspices of the U.S. DOE by  
640 Lawrence Livermore National Laboratory (LLNL) under Contract No. DE-AC52-07NA27344. Efforts of JL, PJG,  
641 MA, AO, PU, KET, PD, CB, MDZ, LC, and BD were supported by the Regional and Global Model Analysis (RGMA)  
642 program of the U.S. Department of Energy (DOE) Office of Science (OS), Biological and Environmental Research  
643 (BER) program. MFW was supported by the Director, OS, BER of the U.S. DOE through the RGMA program under  
644 Contract No. DE340AC02-05CH11231. AGP was supported by U.S. DOE through BER RGMA through Award  
645 Number DE-SC0022070 and via National Science Foundation (NSF) IA 1947282, and by National Center for  
646 Atmospheric Research (NCAR), which is a major facility sponsored by the NSF under Cooperative Agreement No.  
647 1852977. YYP and EG were supported by the Agence Nationale de la Recherche ARISE project, under Grant ANR-  
648 18-CE01-0012, and the Belmont project GOTHAM, under Grant ANR-15-JCLI-0004-01, the European  
649 Commission’s H2020 Programme “Infrastructure for the European Network for Earth System Modelling Phase 3 (IS-  
650 ENES3)” project under Grant Agreement 824084. DK was supported by the New Faculty Startup Fund from Seoul  
651 National University and the KMA R&D program (KMI2022-01313). The authors thank Program Manager Renu  
652 Joseph of the U.S. DOE for the support and advocacy for the Program for Climate Model Diagnosis and  
653 Intercomparison (PCMDI) project and the PMP. We thank Stephen Klein for his leadership for the PCMDI project  
654 from 2019 to 2022. We acknowledge contributions from our LLNL colleagues, Lina Muryanto and Zeshawn Shaheen  
655 (Now at Google LLC) during the early stage of the PMP, and Sasha Ames, Jeff Painter, Chris Mauzey, and Stephen  
656 Po-Chedley for the PCMDI’s CMIP database management. The authors also thank Liping Zhang for her comments  
657 during GFDL’s internal review process.

658

659 **References**

- 660 Adler, R.F., Sapiano, M. R., Huffman, G.J., Wang, J.J., Gu, G., Bolvin, D., Chiu, L., Schneider, U., Becker, A., Nelkin,  
661 E., Xie, P., Ferraro, R., Shin, D.-B.: The Global Precipitation Climatology Project (GPCP) monthly analysis  
662 (new version 2.3) and a review of 2017 global precipitation. *Atmosphere*, 9, 138,  
663 <https://doi.org/10.3390/atmos9040138>, 2018.
- 664 Ahn, M.-S., Kim, D. H., Sperber, K. R., Kang, I.-S., Maloney, E. D., Waliser, D. E., and Hendon, H. H.: MJO  
665 simulation in CMIP5 climate models: MJO skill metrics and process-oriented diagnosis, *Climate Dynamics*,  
666 49, 4023–4045, <https://doi.org/10.1007/s00382-017-3558-4>, 2017.
- 667 Ahn, M.-S., Gleckler, P. J., Lee, J., Pendergrass, A. G., and Jakob, C.: Benchmarking Simulated Precipitation  
668 Variability Amplitude across Time Scales, *Journal of Climate*, 35, 3173–3196, [https://doi.org/10.1175/jcli-](https://doi.org/10.1175/jcli-d-21-0542.1)  
669 [d-21-0542.1](https://doi.org/10.1175/jcli-d-21-0542.1), 2022.



- 670 Ahn, M.-S., Ullrich, P. A., Gleckler, P. J., Lee, J., Ordonez, A. C., and Pendergrass, A. G.: Evaluating precipitation  
671 distributions at regional scales: a benchmarking framework and application to CMIP5 and 6 models,  
672 *Geoscientific Model Development*, 16, 3927–3951, <https://doi.org/10.5194/gmd-16-3927-2023>, 2023.
- 673 Arcodia, M., Barnes, E. A., Mayer, K., Lee, J., Ordonez, A., and Ahn, M.-S.: Assessing decadal variability of  
674 subseasonal forecasts of opportunity using explainable AI, *Environmental Research*,  
675 <https://doi.org/10.1088/2752-5295/aced60>, 2023.
- 676 Ashfaq, M., Rastogi, D., Kitson, J., Abid, M. A., and Kao, S.-C.: Evaluation of CMIP6 GCMs over the CONUS for  
677 downscaling studies, *Journal of Geophysical Research: Atmospheres*, 127, e2022JD036659.  
678 <https://doi.org/10.1029/2022JD036659>, 2022.
- 679 Bayr, T., Wengel, C., Latif, M., Dommenges, D., Lübbecke, J., and Park, W.: Error compensation of ENSO  
680 atmospheric feedbacks in climate models and its influence on simulated ENSO dynamics, *Climate Dynamics*,  
681 53, 155–172, <https://doi.org/10.1007/s00382-018-4575-7>, 2019.
- 682 Biard, J. C. and Kunkel, K. E.: Automated detection of weather fronts using a deep learning neural network, *Adv.  
683 Stat. Clim. Meteorol. Oceanogr.*, 5, 147–160, <https://doi.org/10.5194/ascmo-5-147-2019>, 2019.
- 684 Bellenger, H., Guilyardi, E., Leloup, J., Lengaigne, M., and Vialard, J.: ENSO representation in climate models: from  
685 CMIP3 to CMIP5, *Climate Dynamics*, 42, 1999–2018, <https://doi.org/10.1007/s00382-013-1783-z>, 2013.
- 686 Boucher, O., Servonnat, J., Albright, A. L., Aumont, O., Balkanski, Y., Bastrikov, V., Bekki, S., Bonnet, R., Bony,  
687 S., Bopp, L., Braconnot, P., Brockmann, P., Cadule, P., Caubel, A., Cheruy, F., Codron, F., Cozic, A., Cugnet,  
688 D., D'Andrea, F., Davini, P., De Lavergne, C., Denvil, S., Deshayes, J., Devilliers, M., Ducharme, A.,  
689 Dufresne, J. L., Dupont, E., Ethé, C., Fairhead, L., Falletti, L., Flavoni, S., Foujols, M. A., Gardoll, S.,  
690 Gastineau, G., Ghattas, J., Grandpeix, J. Y., Guenet, B., Lionel, E. G., Guilyardi, E., Guimberteau, M.,  
691 Hauglustaine, D., Hourdin, F., Idelkadi, A., Joussaume, S., Kageyama, M., Khodri, M., Krinner, G., Lebas,  
692 N., Levavasseur, G., Lévy, C., Li, L., Lott, F., Lurton, T., Luyssaert, S., Madec, G., Madeleine, J.-B.,  
693 Maignan, F., Marchand, M., Marti, O., Mellul, L., Meurdesoif, Y., Mignot, J., Musat, I., Ottlé, C., Peylin, P.,  
694 Planton, Y., Polcher, J., Rio, C., Rochetin, N., Rousset, C., Sepulchre, P., Sima, A., Swingedouw, D.,  
695 Thiéblemont, R., Traore, A. K., Vancoppenolle, M., Vial, J., Vialard, J., Viovy, N., and Vuichard, N.:  
696 Presentation and evaluation of the IPSL-CM6A-LR Climate Model, *Journal of Advances in Modeling Earth  
697 Systems*, 12, <https://doi.org/10.1029/2019ms002010>, 2020.
- 698 Caldwell, P., Mamejanov, A., Tang, Q., Van Roekel, L., Golaz, J.-C., Lin, W., Bader, D. C., Keen, N. D., Feng, Y.,  
699 Jacob, R., Maltrud, M., Roberts, A., Taylor, M. A., Veneziani, M., Wang, H., Wolfe, J. D., Balaguru, K.,  
700 Cameron-Smith, P. J., Dong, L., Klein, S. A., Leung, L. R., Li, H., Li, Q., Liu, X., Neale, R., Pinheiro, M.  
701 C., Qian, Y., Ullrich, P. A., Xie, S., Yang, Y., Zhang, Y., Zhang, K., and Zhou, T.: The DOE E3SM Coupled  
702 Model Version 1: description and results at high resolution, *Journal of Advances in Modeling Earth Systems*,  
703 11, 4095–4146, <https://doi.org/10.1029/2019ms001870>, 2019.
- 704 Cannon, A. J.: Reductions in daily continental-scale atmospheric circulation biases between generations of global  
705 climate models: CMIP5 to CMIP6, *Environmental Research Letters*, 15, 064006,  
706 <https://doi.org/10.1088/1748-9326/ab7e4f>, 2020.



- 707 Chen, H.-C., Jin, F.-F., Zhao, S., Wittenberg, A. T., and Xie, S.: ENSO dynamics in the E3SM-1-0, CESM2, and  
708 GFDL-CM4 climate models, *Journal of Climate*, 34, 9365–9384, <https://doi.org/10.1175/JCLI-D-21-0355.1>,  
709 2021.
- 710 Choi, J. H. and Son, S.-W.: Seasonal-to-decadal prediction of El Niño–Southern Oscillation and Pacific Decadal  
711 Oscillation, *Npj Climate and Atmospheric Science*, 5, <https://doi.org/10.1038/s41612-022-00251-9>, 2022.
- 712 Collier, N., Hoffman, F. M., Lawrence, D. M., Keppel-Aleks, G., Koven, C. D., Riley, W. J., Mu, M., and Randerson,  
713 J. T.: The International Land Model Benchmarking (ILAMB) System: Design, theory, and implementation,  
714 *Journal of Advances in Modeling Earth Systems*, 10, 2731–2754, <https://doi.org/10.1029/2018ms001354>,  
715 2018.
- 716 Covey, C., AchutaRao, K., Cubasch, U., Jones, P., Lambert, S. J., Mann, M., Phillips, T. J., and Taylor, K. E.: An  
717 overview of results from the Coupled Model Intercomparison Project, *Global and Planetary Change*, 37, 103–  
718 133, [https://doi.org/10.1016/s0921-8181\(02\)00193-5](https://doi.org/10.1016/s0921-8181(02)00193-5), 2003.
- 719 Covey, C., Gleckler, P. J., Doutriaux, C., Williams, D. N., Dai, A., Fasullo, J. T., Trenberth, K. E., and Berg, A.:  
720 Metrics for the diurnal cycle of precipitation: toward routine benchmarks for climate models, *Journal of*  
721 *Climate*, 29, 4461–4471, <https://doi.org/10.1175/jcli-d-15-0664.1>, 2016.
- 722 Crockford, D.: The application/json media type for javascript object notation (json) (No. rfc4627), [https://www.rfc-](https://www.rfc-editor.org/rfc/pdf/rfc4627.txt.pdf)  
723 [editor.org/rfc/pdf/rfc4627.txt.pdf](https://www.rfc-editor.org/rfc/pdf/rfc4627.txt.pdf) (last access: 6 November 2023), 2006.
- 724 Crockford, D. and Morningstar, C.: The JSON Data Interchange Syntax, ECMA-404, ECMA International, 2017.
- 725 Dalelane, C., Winderlich, K., and Walter, A.: Evaluation of global teleconnections in CMIP6 climate projections using  
726 complex networks, *Earth Syst. Dynam.*, 14, 17–37, <https://doi.org/10.5194/esd-14-17-2023>, 2023.
- 727 Dee, D. P., Uppala, S. M., Simmons, A. J., Berrisford, P., Poli, P., Kobayashi, S., Andrae, U., Balmaseda, M. A.,  
728 Balsamo, G., Bauer, P., Bechtold, P., Beljaars, A. C. M., van de Berg, L., Bidlot, J., Bormann, N., Delsol,  
729 C., Dragani, R., Fuentes, M., Geer, A. J., Haimberger, L., Healy, S. B., Hersbach, H., Hólm, E. V., Isaksen,  
730 L., Källberg, P., Köhler, M., Matricardi, M., McNally, A. P., Monge-Sanz, B. M., Morcrette, J.-J., Park, B.-  
731 K., Peubey, C., de Rosnay, P., Tavolato, C., Thépaut, J.-N., and Vitart, F.: The ERA-Interim reanalysis:  
732 Configuration and performance of the data assimilation system, *Quarterly Journal of the Royal*  
733 *Meteorological Society*, 137, 553–597, <https://doi.org/10.1002/qj.828>, 2011
- 734 Deser, C. and Phillips, A. S.: Defining the internal component of Atlantic multidecadal variability in a changing  
735 climate, *Geophysical Research Letters*, 48, <https://doi.org/10.1029/2021gl095023>, 2021.
- 736 Doutriaux, C., Nadeau, D., Wittenburg, S., Lipsa, D., Muryanto, L., Chaudhary, A., and Williams, D. N.: CDAT/cdat:  
737 CDAT 8.1, Zenodo [Code], <https://doi.org/10.5281/zenodo.2586088>, 2019.
- 738 Durack, P. J., Taylor, K. E., Eyring, V., Ames, S., Hoang, T., Nadeau, D., Doutriaux, C., Stockhouse, M., and Gleckler,  
739 P. J.: Toward standardized data sets for climate model experimentation, *Eos, Transactions American*  
740 *Geophysical Union*, 99, <https://doi.org/10.1029/2018eo101751>, 2018.
- 741 Eaton, B., Gregory, J., Drach, B., Taylor, K., Hankin, S., Blower, J., Caron, J., Signell, R., Bentley, P., Rappa, G.,  
742 Höck, H., Pamment, A., Juckes, M., Raspaud, M., Horne, R., Whiteaker, T., Blodgett, D., Zender, C., Lee,  
743 D., Hassell, D., Snow, A. D., Kölling, T., Allured, D., Jelenak, A., Soerensen, A. M., Gaultier, L., Herlédan,



- 744 S.: NetCDF Climate and Forecast (CF) Meta-data Conventions V1.10, available at:  
745 <http://cfconventions.org/Data/cf-conventions/cf-conventions-1.10/cf-conventions.html> (last access: 6  
746 November 2023), 2022.
- 747 Eyring, V., Righi, M., Lauer, A., Evaldsson, M., Wenzel, S., Jones, C., Anav, A., Andrews, O., Cionni, I., Davin, E.  
748 L., Deser, C., Ehbrecht, C., Friedlingstein, P., Gleckler, P. J., Gottschaldt, K.-D., Hagemann, S., Juckes, M.,  
749 Kindermann, S., Krasting, J. P., Kunert, D., Levine, R. C., Loew, A., Mäkelä, J., Martin, G., Mason, E.,  
750 Phillips, A. S., Read, S., Rio, C., Roehrig, R., Senftleben, D., Sterl, A., Van Ulft, L. H., Walton, J., Wang,  
751 S., and Williams, K. D.: ESMValTool (v1.0) – a community diagnostic and performance metrics tool for  
752 routine evaluation of Earth system models in CMIP, *Geoscientific Model Development*, 9, 1747–1802,  
753 <https://doi.org/10.5194/gmd-9-1747-2016>, 2016a.
- 754 Eyring, V., Bony, S., Meehl, G. A., A. C., Senior, Stevens, B., Stouffer, R. J., and Taylor, K. E.: Overview of the  
755 Coupled Model Intercomparison Project Phase 6 (CMIP6) experimental design and organization,  
756 *Geoscientific Model Development*, 9, 1937–1958, <https://doi.org/10.5194/gmd-9-1937-2016>, 2016b.
- 757 Eyring, V., Cox, P. M., Flato, G. M., Gleckler, P. J., Abramowitz, G., Caldwell, P., Collins, W. D., Gier, B. K., Hall,  
758 A., Hoffman, F. M., Hurtt, G. C., Jahn, A., Jones, C. D., Klein, S. A., Krasting, J. P., Kwiatkowski, L.,  
759 Lorenz, R., Maloney, E. D., Meehl, G. A., Pendergrass, A. G., Pincus, R., Ruane, A. C., Russell, J. L.,  
760 Sanderson, B. M., Santer, B. D., Sherwood, S. C., Simpson, I. R., Stouffer, R. J., and Williamson, M. S.:  
761 Taking climate model evaluation to the next level, *Nature Climate Change*, 9, 102–110,  
762 <https://doi.org/10.1038/s41558-018-0355-y>, 2019.
- 763 Eyring, V., Bock, L., Lauer, A., Righi, M., Schlund, M., Andela, B., Arnone, E., Bellprat, O., Brötz, B., Caron, L.-P.,  
764 Carvalhais, N., Cionni, I., Cortesi, N., Crezee, B., Davin, E. L., Davini, P., Debeire, K., De Mora, L., Deser,  
765 C., Docquier, D., Earnshaw, P., Ehbrecht, C., Gier, B. K., Gonzalez-Reviriego, N., Goodman, P. J.,  
766 Hagemann, S., Hardiman, S. C., Hassler, B., Hunter, A., Kadow, C., Kindermann, S., Koirala, S., Koldunov,  
767 N., Lejeune, Q., Lembo, V., Lovato, T., Lucarini, V., Massonnet, F., Müller, B., Pandde, A., Pérez-Zanón,  
768 N., Phillips, A. S., Predoi, V., Russell, J. L., Sellar, A., Serva, F., Stacke, T., Swaminathan, R., Torralba, V.,  
769 Vegas-Regidor, J., Von Hardenberg, J., Weigel, K., and Zimmermann, K.: Earth System Model Evaluation  
770 Tool (ESMValTool) v2.0 – an extended set of large-scale diagnostics for quasi-operational and  
771 comprehensive evaluation of Earth system models in CMIP, *Geoscientific Model Development*, 13, 3383–  
772 3438, <https://doi.org/10.5194/gmd-13-3383-2020>, 2020.
- 773 Eyring, V., Gillett, N.P., Achuta Rao, K.M., Barimalala, R., Barreiro Parrillo, M., Bellouin, N., Cassou, C., Durack,  
774 P.J., Kosaka, Y., McGregor, S. and Min, S., Morgenstern, O., and Sun, Y.: Human Influence on the Climate  
775 System. In *Climate Change 2021: The Physical Science Basis. Contribution of Working Group I to the Sixth*  
776 *Assessment Report of the Intergovernmental Panel on Climate Change*. 105, 423–552,  
777 <https://doi.org/10.1017/9781009157896.005>, 2021.
- 778 Fasullo, J. T.: Evaluating simulated climate patterns from the CMIP archives using satellite and reanalysis datasets  
779 using the Climate Model Assessment Tool (CMATv1), *Geoscientific Model Development*, 13, 3627–3642,  
780 <https://doi.org/10.5194/gmd-13-3627-2020>, 2020.



- 781 Fasullo, J. T., Phillips, A. S., and Deser, C.: Evaluation of leading modes of climate variability in the CMIP archives,  
782 *Journal of Climate*, 33, 5527–5545, <https://doi.org/10.1175/jcli-d-19-1024.1>, 2020.
- 783 Ferraro, R., Waliser, D. E., Gleckler, P. J., Taylor, K. E., and Eyring, V.: Evolving OBS4MIPS to support Phase 6 of  
784 the Coupled Model Intercomparison Project (CMIP6), *Bulletin of the American Meteorological Society*,  
785 <https://doi.org/10.1175/bams-d-14-00216.1>, 2015.
- 786 Flato, G., Marotzke, J., Abiodun, B., Braconnot, P., Chou, S.C., Collins, W., Cox, P., Driouech, F., Emori, S., Eyring,  
787 V. and Forest, C.: Evaluation of climate models. In *Climate change 2013: the physical science basis. Contribution of Working Group I to the Fifth Assessment Report of the Intergovernmental Panel on Climate Change* (pp. 741-866). Cambridge University Press. 2014.
- 788  
789
- 790 Fu, W., Moore, J. K., Primeau, F., Collier, N., Ogunro, O. O., Hoffman, F. M. and Randerson, J. T.: Evaluation of  
791 ocean biogeochemistry and carbon cycling in CMIP earth system models with the international ocean model  
792 benchmarking (IOMB) software System. *Journal of Geophysical Research: Oceans*, 127, e2022JC018965,  
793 <https://doi.org/10.1029/2022JC018965>, 2022.
- 794 Gates, W.L.: AN AMS continuing series: Global CHANGE–AMIP: The atmospheric model intercomparison project,  
795 *Bulletin of the American Meteorological Society*, 73, 1962-1970, 1992.
- 796 Gates, W.L., Henderson-Sellers, A., Boer, G.J., Folland, C.K., Kitoh, A., McAvaney, B.J., Semazzi, F., Smith, N.,  
797 Weaver, A.J. and Zeng, Q.C.: Climate models—evaluation. *Climate change* 1: 229-284, 1995.
- 798 Gates, W.L., Boyle, J.S., Covey, C., Dease, C.G., Doutriaux, C.M., Drach, R.S., Fiorino, M., Gleckler, P.J., Hnilo,  
799 J.J., Marlais, S.M. and Phillips, T.J.: An overview of the results of the Atmospheric Model Intercomparison  
800 Project (AMIP I). *Bulletin of the American Meteorological Society*, 80, 29-56, 1999.
- 801 Gleckler, P. J., Taylor, K. E., and Doutriaux, C.: Performance metrics for climate models, *Journal of Geophysical*  
802 *Research*, 113, <https://doi.org/10.1029/2007jd008972>, 2008.
- 803 Gleckler, P. J., Ferraro, R., and Waliser, D. E.: Improving use of satellite data in evaluating climate models, *Eos*,  
804 *Transactions American Geophysical Union*, 92, 172, <https://doi.org/10.1029/2011eo200005>, 2011.
- 805 Gleckler, P. J., Doutriaux, C., Durack, P. J., Taylor, K. E., Zhang, Y., Williams, D. N., Mason, E., and Servonnat, J.:  
806 A more powerful reality test for climate models, *Eos, Transactions American Geophysical Union*, 97,  
807 <https://doi.org/10.1029/2016eo051663>, 2016.
- 808 Golaz, J.-C., Caldwell, P., Van Roekel, L., Petersen, M. R., Tang, Q., Wolfe, J. D., Abeshu, G. W., Anantharaj, V.,  
809 Asay-Davis, X., Bader, D. C., Baldwin, S., Bisht, G., Bogenschutz, P., Branstetter, M. L., Brunke, M. A.,  
810 Brus, S., Burrows, S. M., Cameron-Smith, P. J., Donahue, A. S., Deakin, M., Easter, R. C., Evans, K. J.,  
811 Feng, Y., Flanner, M., Foucar, J. G., Fyke, J., Griffin, B. M., Hannay, C., Harrop, B. E., Hoffman, M. J.,  
812 Hunke, E., Jacob, R., Jacobsen, D. W., Jeffery, N., Jones, P. W., Keen, N. D., Klein, S. A., Larson, V. E.,  
813 Leung, L. R., Li, H. Y., Lin, W., Lipscomb, W. H., Lun, P., Mahajan, S., Maltrud, M., Mamejtanov, A.,  
814 McClean, J. L., McCoy, R., Neale, R., Price, S., Qian, Y., Rasch, P. J., Eyre, J. E. J. R., Riley, W. J., Ringler,  
815 T. D., Roberts, A., Roesler, E. L., Salinger, A. G., Shaheen, Z., Shi, X., Singh, B., Tang, J., Taylor, M. A.,  
816 Thornton, P. E., Turner, A. K., Veneziani, M., Wan, H., Wang, H., Wang, S., Williams, D. N., Wolfram, P.  
817 J., Worley, P. H., Xie, S., Yang, Y., Yoon, J., Zelinka, M. D., Zender, C. S., Zeng, X., Zhang, C., Zhang, K.,



- 818 Zhang, Y., Zheng, X., Zhou, T., and Zhu, Q.: The DOE E3SM Coupled Model Version 1: Overview and  
819 evaluation at standard resolution, *Journal of Advances in Modeling Earth Systems*, 11, 2089–2129,  
820 <https://doi.org/10.1029/2018ms001603>, 2019.
- 821 Goldenson, N., Leung, L. R., Mearns, L. O., Pierce, D. W., Reed, K. A., Simpson, I. R., Ullrich, P., Krantz, W., Hall,  
822 A., Jones, A. and Rahimi, S.: Use-Inspired, Process-Oriented GCM Selection: Prioritizing Models for  
823 Regional Dynamical Downscaling, *Bulletin of the American Meteorological Society*, E1619–E1629,  
824 <https://doi.org/10.1175/BAMS-D-23-0100.1>, 2023.
- 825 Guilyardi, E., Wittenberg, A., Fedorov, A., Collins, M., Wang, C., Capotondi, A., Van Oldenborgh, G.J. and  
826 Stockdale, T.: Understanding El Niño in ocean–atmosphere general circulation models: Progress and  
827 challenges, *Bulletin of the American Meteorological Society*, 90, 325–340,  
828 <https://doi.org/10.1175/2008BAMS2387.1>, 2009.
- 829 Guilyardi E., Capotondi, A., Lengaigne, M., Thual, S., Wittenberg, A. T.: ENSO modelling: history, progress and  
830 challenges, in: *El Niño in a changing climate*, edited by: McPhaden, M. J., Santoso, A., Cai, W., AGU  
831 monograph, ISBN: 9781119548164, <https://doi.org/10.1002/9781119548164.ch9>, 2020.
- 832 Haarsma, R. J., Roberts, M., Vidale, P. L., A, C., Senior, Bellucci, A., Bao, Q., Chang, P., Corti, S., Fučkar, N. S.,  
833 Guemas, V., Von Hardenberg, J., Hazeleger, W., Kodama, C., Koenigk, T., Leung, L. R., Lu, J., Luo, J.,  
834 Mao, J., Mizielinski, M. S., Mizuta, R., Nobre, P., Satoh, M., Scoccimarro, E., Semmler, T., Small, R. J., and  
835 Von Storch, J. S.: High Resolution Model Intercomparison Project (HiGHRESMIP v1.0) for CMIP6,  
836 *Geoscientific Model Development*, 9, 4185–4208, <https://doi.org/10.5194/gmd-9-4185-2016>, 2016.
- 837 Hintze, J. L., and Nelson, R. D.: Violin plots: A box plot-density trace synergism, *The American Statistician*, 52, 181–  
838 184, <https://doi.org/10.1080/00031305.1998.10480559>, 1998.
- 839 Hannah, W. M., Bradley, A. M., Guba, O., Tang, Q., Golaz, J.-C., and Wolfe, J. D.: Separating physics and dynamics  
840 grids for improved computational efficiency in spectral element Earth system models, *Journal of Advances  
841 in Modeling Earth Systems*, 13, <https://doi.org/10.1029/2020ms002419>, 2021.
- 842 Hassan, K. A., Rönnerberg, N., Forsell, C., Cooper, M. and Johansson, J.: A study on 2D and 3D parallel coordinates  
843 for pattern identification in temporal multivariate data, in: 2019 23rd International Conference Information  
844 Visualisation (IV), 145–150, <https://doi.org/10.1109/IV.2019.00033>, 2019.
- 845 Hassell, D., Gregory, J. M., Blower, J., Lawrence, B., and Taylor, K. E.: A data model of the Climate and Forecast  
846 metadata conventions (CF-1.6) with a software implementation (cf-python v2.1), *Geoscientific Model  
847 Development*, 10, 4619–4646, <https://doi.org/10.5194/gmd-10-4619-2017>, 2017.
- 848 Hausfather, Z., Marvel, K., Schmidt, G. A., Nielsen-Gammon, J. W. and Zelinka, M.: Climate simulations: Recognize  
849 the ‘hot model’ problem, *Nature*, 605, 26–29, <https://doi.org/10.1038/d41586-022-01192-2>, 2022.
- 850 Held, I. M., Guo, H., Adcroft, A., Dunne, J. P., Horowitz, L. W., Krasting, J., Shevliakova, E., Winton, M., Zhao, M.,  
851 Bushuk, M., Wittenberg, A. T., and coauthors: Structure and performance of GFDL's CM4. 0 climate model,  
852 *Journal of Advances in Modeling Earth Systems*, 11, 3691–3727, <https://doi.org/10.1029/2019MS001829>,  
853 2019.





- 854 Hendon, H. H., Zhang, C., and Glick, J. D.: Interannual Variation of the Madden–Julian Oscillation during Austral  
855 Summer, *Journal of Climate*, 12, 2538–2550, 1999.
- 856 Herger, N., Abramowitz, G., Knutti, R., Angéilil, O., Lehmann, K., and Sanderson, B. M.: Selecting a climate model  
857 subset to optimise key ensemble properties, *Earth System Dynamics Discussions*, 9, 135–151,  
858 <https://doi.org/10.5194/esd-9-135-2018>, 2018.
- 859 Hersbach, H., Bell, B., Berrisford, P., Hirahara, S., Horányi, A., Muñoz-Sabater, J., Nicolas, J., Peubey, C., Radu, R.,  
860 Schepers, D. and coauthors: The ERA5 global reanalysis. *Quarterly Journal of the Royal Meteorological*  
861 *Society*, 146, 1999–2049, <https://doi.org/10.1002/qj.3803>, 2020.
- 862 Huffman, G. J., Adler, R. F., Morrissey, M. M., Bolvin, D. T., Curtis, S., Joyce, R., McGavock, B. and Susskind, J.:  
863 Global precipitation at one-degree daily resolution from multisatellite observations, *Journal of*  
864 *hydrometeorology*, 2, 36–50, 2001.
- 865 Huffman, G. J., Bolvin, D. T., Braithwaite, D., Hsu, K., Joyce, R., Kidd, C., Nelkin, E. J., Sorooshian, S., Tan, J., and  
866 Xie, P.: NASA global precipitation measurement (GPM) integrated multi-satellite retrievals for GPM  
867 (IMERG). Algorithm theoretical basis document (ATBD) version, 4, p.30., 2015.
- 868 Inselberg, A.: Multidimensional detective, in: *Proceedings of IEEE Symposium on Information Visualization*, 100–  
869 107, <https://doi.org/10.1109/INFVIS.1997.636793>, 1997.
- 870 Inselberg, A.: Parallel Coordinates: Visualization, Exploration and Classification of High-Dimensional Data, in:  
871 *Handbook of Data Visualization*, edited by Chen, C., Härdle, W., and Unwin, A., Springer, Berlin,  
872 Heidelberg, Germany, 643–680, [https://doi.org/10.1007/978-3-540-33037-0\\_25](https://doi.org/10.1007/978-3-540-33037-0_25), 2008.
- 873 Inselberg, A.: Parallel Coordinates, in: *Encyclopedia of Database Systems*. Springer, edited by Liu, L., and Özsu, M.  
874 T., Springer, New York, NY, U.S.A., [https://doi.org/10.1007/978-1-4899-7993-3\\_262-2](https://doi.org/10.1007/978-1-4899-7993-3_262-2), 2016.
- 875 Johansson, J. and Forsell, C.: Evaluation of parallel coordinates: Overview, categorization and guidelines for future  
876 research, *IEEE Transactions on Visualization and Computer Graphics*, 22, 579–588,  
877 <https://doi.org/10.1109/TVCG.2015.2466992>, 2016.
- 878 Jakob, C., Gettelman, A. and Pitman, A.: The need to operationalize climate modelling, *Nat. Clim. Chang.* 13, 1158–  
879 1160, <https://doi.org/10.1038/s41558-023-01849-4>, 2023.
- 880 Joyce, R. J., Janowiak, J. E., Arkin, P. A. and Xie, P.: CMORPH: A method that produces global precipitation  
881 estimates from passive microwave and infrared data at high spatial and temporal resolution, *Journal of*  
882 *hydrometeorology*, 5, 487–503, 2004.
- 883 Jun, S.-Y., Kim, J.-H., Choi, J. H., Kim, S.-J., Kim, B.-M., and An, S.-I.: The internal origin of the west-east  
884 asymmetry of Antarctic climate change, *Science Advances*, 6, <https://doi.org/10.1126/sciadv.aaz1490>, 2020.
- 885 Kang, D., Kim, D. H., Ahn, M.-S., Neale, R., Lee, J., and Gleckler, P. J.: The role of the mean state on MJO simulation  
886 in CESM2 ensemble simulation, *Geophysical Research Letters*, 47, <https://doi.org/10.1029/2020gl089824>,  
887 2020.
- 888 Kim, D., Sperber, K. R., Stern, W., Waliser, D. E., Kang, I. S., Maloney, E. D., Wang, W., Weickmann, K. M.,  
889 Benedict, J. J., Khairoutdinov, M., Lee, M.-I., Neale, R., Suarez, M. J., Thayer-Calder, K., and Zhang, G.:



- 890 Application of MJO simulation diagnostics to climate models, *Journal of Climate*, 22, 6413–6436,  
891 <https://doi.org/10.1175/2009jcli3063.1>, 2009.
- 892 Kim, H., Caron, J. M., Richter, J. H. and Simpson, I. R.: The lack of QBO-MJO connection in CMIP6 models,  
893 *Geophysical Research Letters*, 47, e2020GL087295, <https://doi.org/10.1029/2020GL087295>, 2020.
- 894 Kim, Y.-H., Min, S.-K., Zhang, X., Sillmann, J., and Sandstad, M.: Evaluation of the CMIP6 multi-model ensemble  
895 for climate extreme indices, *Weather and Climate Extremes*, 29, 100269,  
896 <https://doi.org/10.1016/j.wace.2020.100269>, 2020.
- 897 Klein, S. A., Zhang, Y., Zelinka, M. D., Pincus, R., Boyle, J., and Gleckler, P. J.: Are climate model simulations of  
898 clouds improving? An evaluation using the ISCCP simulator, *Journal of Geophysical Research:*  
899 *Atmospheres*, 118, 1329–1342, <https://doi.org/10.1002/jgrd.50141>, 2013.
- 900 Klingaman, N. P., Martin, G., and Moise, A.: ASoP (v1.0): a set of methods for analyzing scales of precipitation in  
901 general circulation models, *Geoscientific Model Development*, 10, 57–83, [https://doi.org/10.5194/gmd-10-](https://doi.org/10.5194/gmd-10-57-2017)  
902 [57-2017](https://doi.org/10.5194/gmd-10-57-2017), 2017.
- 903 Knutti, R.: The end of model democracy? *Climatic Change*, 102, 395–404, [https://doi.org/10.1007/s10584-010-9800-](https://doi.org/10.1007/s10584-010-9800-2)  
904 [2](https://doi.org/10.1007/s10584-010-9800-2), 2010.
- 905 Knutti, R., Sedláček, J., Sanderson, B. M., Lorenz, R., Fischer, E. M., and Eyring, V.: A climate model projection  
906 weighting scheme accounting for performance and interdependence, *Geophysical Research Letters*,  
907 <https://doi.org/10.1002/2016gl072012>, 2017.
- 908 Knutti, R., Abramowitz, G., Collins, M., Eyring, V., Gleckler, P. J., Hewitson, B., and Mearns, L.: Good Practice  
909 Guidance Paper on Assessing and Combining Multi Model Climate Projections, in: Meeting Report of the  
910 Intergovernmental Panel on Climate Change Expert Meeting on Assessing and Combining Multi Model  
911 Climate Projections, edited by Stocker, T. F., Qin, D., Plattner, G.-K., Tignor, M., and Midgley, P. M., IPCC  
912 Working Group I Technical Support Unit, University of Bern, Bern, Switzerland, 2010.
- 913 Labe, Z. M. and Barnes, E. A.: Comparison of Climate Model Large Ensembles With Observations in the Arctic Using  
914 Simple Neural Networks, *Earth and Space Science*, e2022EA002348,  
915 <https://doi.org/10.1029/2022EA002348>, 2022.
- 916 Lambert, S. J. and Boer, G. J.: CMIP1 evaluation and intercomparison of coupled climate models, *Climate Dynamics*,  
917 17, 83–106, <https://doi.org/10.1007/PL00013736>, 2001.
- 918 Lee, H., Goodman, A., McGibbney, L. J., Waliser, D. E., Kim, J., Loikith, P. C., Gibson, P. B., and Massoud, E.:  
919 Regional Climate Model Evaluation System powered by Apache Open Climate Workbench v1.3.0: an  
920 enabling tool for facilitating regional climate studies, *Geoscientific Model Development*, 11, 4435–4449,  
921 <https://doi.org/10.5194/gmd-11-4435-2018>, 2018a.
- 922 Lee, J., Ahn, M.-S., Ordonez, A., Gleckler, P., and Ullrich, P.: PCMDI/pcmdi\_metrics\_results\_archive, Zenodo [data],  
923 <https://doi.org/10.5281/zenodo.10181201>, 2023a.
- 924 Lee, J., Gleckler, P., Ordonez, A., Ahn, M.-S., Ullrich, P., Tom, V., Jason, B., Charles, D., Durack, P., Shaheen, Z.,  
925 Muryanto, L., Painter, J., and Krasting, J.: PCMDI/pcmdi\_metrics: PMP Version 3.1.1, Zenodo [code],  
926 <https://doi.org/10.5281/zenodo.592790>, 2023b.



- 927 Lee, J., Gleckler, P., Sperber, K., Doutriaux C., and Williams, D.: High-dimensional Data Visualization for Climate  
928 Model Intercomparison: Application of the Circular Plot, in: Proceedings of the 8th International Workshop  
929 on Climate Informatics: CI 2018. NCAR Technical Note NCAR/TN-550+PROC, 12-14,  
930 <http://dx.doi.org/10.5065/D6BZ64XQ>, 2018b.
- 931 Lee, J., Planton, Y., Gleckler, P. J., Sperber, K. R., Guilyardi, E., Wittenberg, A. T., McPhaden, M. J., and Pallotta,  
932 G.: Robust evaluation of ENSO in climate models: How many ensemble members are needed?, *Geophysical*  
933 *Research Letters*, 48, <https://doi.org/10.1029/2021gl095041>, 2021a.
- 934 Lee, J., Sperber, K. R., Gleckler, P. J., Bonfils, C., and Taylor, K. E.: Quantifying the agreement between observed  
935 and simulated extratropical modes of interannual variability, *Climate Dynamics*, 52, 4057–4089,  
936 <https://doi.org/10.1007/s00382-018-4355-4>, 2019a.
- 937 Lee, J., Sperber, K. R., Gleckler, P. J., Taylor, K. E., and Bonfils, C.: Benchmarking performance changes in the  
938 simulation of extratropical modes of variability across CMIP generations, *Journal of Climate*, 1–70,  
939 <https://doi.org/10.1175/jcli-d-20-0832.1>, 2021b.
- 940 Lee, J., Xue, Y., De Sales, F., Diallo, I., Marx, L., Ek, M., Sperber, K. R., and Gleckler, P. J.: Evaluation of multi-  
941 decadal UCLA-CFSv2 simulation and impact of interactive atmospheric-ocean feedback on global and  
942 regional variability, *Climate Dynamics*, 52, 3683–3707, <https://doi.org/10.1007/s00382-018-4351-8>, 2019b.
- 943 Leung, L. R., Boos, W. R., Catto, J. L., DeMott, C. A., Martin, G. M., Neelin, J. D., O'Brien, T. A., Xie, S., Feng, Z.,  
944 Klingaman, N. P. Kuo, Y.-H., Lee, R. W., Martinez-Villalobos, C., Vishnu S., Priestley, M. D. K., Tao, C.,  
945 and Zhou, Y.: Exploratory precipitation metrics: Spatiotemporal characteristics, process-oriented, and  
946 phenomena-based, *Journal of Climate*, 35, <https://doi.org/10.1175/JCLI-D-21-0590.1>, 3659-3686, 2022.
- 947 Lin, J.-P., Kiladis, G. N., Mapes, B. E., Weickmann, K. M., Sperber, K. R., Lin, W., Wheeler, M. C., Schubert, S. D.,  
948 Del Genio, A. D., Donner, L. J., Emori, S., Guérémy, J.-F., Hourdin, F., Rasch, P. J., Roegner, E., and  
949 Scinocca, J.: Tropical intraseasonal variability in 14 IPCC AR4 climate Models. Part I: Convective Signals,  
950 *Journal of Climate*, 19, 2665–2690, <https://doi.org/10.1175/jcli3735.1>, 2006.
- 951 Lin, Y., Huang, X., Liang, Y., Qin, Y., Xu, S., Huang, W., Xu, F., Liu, L., Wang, Y., Peng, Y. and Wang, L.:  
952 Community integrated earth system model (CIESM): Description and evaluation, *Journal of Advances in*  
953 *Modeling Earth Systems*, 12, <https://doi.org/10.1029/2019ms002036>, 2020.
- 954 Loeb, N. G., Doelling, D. R., Wang, H., Su, W., Nguyen, C., Corbett, J. G., Liang, L., Mitrescu, C., Rose, F. G., and  
955 Seiji, K.: Clouds and the Earth's Radiant Energy System (CERES) Energy Balanced and Filled (EBAF) top-  
956 of-atmosphere (TOA) Edition-4.0 data product, *International Journal of Climatology*, 31, 895–918,  
957 <https://doi.org/10.1175/JCLI-D-17-0208.1>, 2018.
- 958 Longmate, J. M., Risser, M. D. and Feldman, D. R.: Prioritizing the selection of CMIP6 model ensemble members for  
959 downscaling projections of CONUS temperature and precipitation, *Clim Dyn* 61, 5171–5197,  
960 <https://doi.org/10.1007/s00382-023-06846-z>, 2023.
- 961 Lu, L., Wang, W. and Tan, Z.: Double-arc parallel coordinates and its axes re-ordering methods, *Mobile Networks*  
962 *and Applications*, 25, 1376-1391, <https://doi.org/10.1007/s11036-019-01455-9>, 2020.



- 963 Madden, R. A. and Julian, P.: Detection of a 40–50 day oscillation in the zonal wind in the Tropical Pacific, *Journal*  
964 *of the Atmospheric Sciences*, 28, 702–708, [https://doi.org/10.1175/1520-0469\(1971\)028](https://doi.org/10.1175/1520-0469(1971)028), 1971.
- 965 Madden, R. A. and Julian, P.: Description of Global-Scale Circulation Cells in the Tropics with a 40–50 Day Period,  
966 *Journal of the Atmospheric Sciences*, 29, 1109–1123, [https://doi.org/10.1175/1520-0469\(1972\)029](https://doi.org/10.1175/1520-0469(1972)029), 1972.
- 967 Madden, R. A. and Julian, P.: Observations of the 40–50-Day Tropical Oscillation—A Review, *Monthly Weather*  
968 *Review*, 122, 814–837, [https://doi.org/10.1175/1520-0493\(1994\)122](https://doi.org/10.1175/1520-0493(1994)122), 1994.
- 969 Martin, G. M., Klingaman, N. P., and Moise, A. F.: Connecting spatial and temporal scales of tropical precipitation in  
970 observations and the MetUM-GA6, *Geoscientific Model Development*, 10, 105–126,  
971 <https://doi.org/10.5194/gmd-10-105-2017>, 2017.
- 972 Maloney, E. D., Gettelman, A., Ming, Y., Neelin, J. D., Barrie, D., Mariotti, A., Chen, C., Coleman, D., Kuo, Y. H.,  
973 Singh, B., Annamalai, H., Berg, A., Booth, J. F., Camargo, S. J., Dai, A., Gonzalez, A., Hafner, J., Jiang, X.,  
974 Jing, X., Kim, D. H., Kumar, A., Moon, Y., Naud, C. M., Sobel, A. H., Suzuki, K., Wang, F., Wang, J., Wing,  
975 A. A., Xu, X., and Zhao, M.: Process-Oriented evaluation of climate and weather forecasting models, *Bulletin*  
976 *of the American Meteorological Society*, 100, 1665–1686, <https://doi.org/10.1175/bams-d-18-0042.1>, 2019.
- 977 McAvaney, B.J., Covey, C., Joussaume, S., Kattsov, V., Kitoh, A., Ogana, W., Pitman, A.J., Weaver, A.J., Wood,  
978 R.A. and Zhao, Z.C.: Model evaluation. In *Climate Change 2001: The scientific basis. Contribution of WG1*  
979 *to the Third Assessment Report of the IPCC (TAR) 471-523*, Cambridge University Press, 2001.
- 980 McPhaden, M. J., Zebiak, S. E., and Glantz, M. H.: ENSO as an integrating concept in Earth Science, *Science*, 314,  
981 1740–1745, <https://doi.org/10.1126/science.1132588>, 2006.
- 982 McPhaden, M. J., Santoso, A., Cai, W. (Eds.): *El Niño Southern oscillation in a changing climate*, American  
983 *Geophysical Union*, USA, 528 pp., ISBN:9781119548126, <https://doi.org/10.1002/9781119548164>, 2020.
- 984 Mears, C. A., Smith, D. K., Ricciardulli, L., Wang, J., Huelsing, H., & Wentz, F. J.: Construction and uncertainty  
985 estimation of a satellite-derived total precipitable water data record over the world's oceans, *Earth and Space*  
986 *Science*, 5, 197–210, <https://doi.org/10.1002/2018EA000363>, 2018.
- 987 Meehl, G. A., Boer, G. J., Covey, C., Latif, M., and Stouffer, R. J.: The Coupled Model Intercomparison Project  
988 (CMIP), *Bulletin of the American Meteorological Society*, 81, 313–318, 2000.
- 989 Meehl, G. A., Boer, G. J., Covey, C., Latif, M., and Stouffer, R. J.: Intercomparison makes for a better climate model,  
990 *Eos, Transactions American Geophysical Union*, 78, 445, <https://doi.org/10.1029/97eo00276>, 1997.
- 991 Meehl, G. A., Covey, C., Delworth, T. L., Latif, M., McAvaney, B. J., Mitchell, J. F. B., Stouffer, R. J., and Taylor,  
992 K. E.: THE WCRP CMIP3 Multimodel Dataset: A new era in climate change research, *Bulletin of the*  
993 *American Meteorological Society*, 88, 1383–1394, <https://doi.org/10.1175/bams-88-9-1383>, 2007.
- 994 Merrifield, A., Brunner, L., Lorenz, R., Humphrey, V., and Knutti, R.: Climate model Selection by Independence,  
995 Performance, and Spread (ClimSIPS v1.0.1) for regional applications, *Geoscientific Model Development*,  
996 16, 4715–4747, <https://doi.org/10.5194/gmd-16-4715-2023>, 2023.
- 997 Neelin, J. D., Krasting, J. P., Radhakrishnan, A., Liptak, J., Jackson, T. J., Ming, Y., Dong, W., Gettelman, A.,  
998 Coleman, D., Maloney, E. D., Wing, A. A., Kuo, Y. H., Ahmed, F., Ullrich, P. A., Bitz, C. M., Neale, R.,  
999 Ordonez, A., and Maroon, E.: Process-oriented diagnostics: principles, practice, community development



1000 and common standards, *Bulletin of the American Meteorological Society*, [https://doi.org/10.1175/bams-d-](https://doi.org/10.1175/bams-d-21-0268.1)  
1001 21-0268.1, 2023.

1002 Nowack, P., Runge, J., Eyring, V., and Haigh, J. D.: Causal networks for climate model evaluation and constrained  
1003 projections, *Nature Communications*, 11, <https://doi.org/10.1038/s41467-020-15195-y>, 2020.

1004 Orbe, C., Van Roekel, L., Adames, Á. F., Dezfuli, A., Fasullo, J. T., Gleckler, P. J., Lee, J., Li, W., Nazarenko, L.,  
1005 Schmidt, G. A., Sperber, K. R., and Zhao, M.: Representation of modes of variability in six U.S. climate  
1006 models, *Journal of Climate*, 33, 7591–7617, <https://doi.org/10.1175/jcli-d-19-0956.1>, 2020.

1007 Ordonez, A. C., Klingaman, N. P., and Martin, G.: Analysing scales of precipitation, OSTI OAI (U.S. Department of  
1008 Energy Office of Scientific and Technical Information), <https://doi.org/10.11578/dc.20211029.5>, 2021.

1009 Papalexiou, S. M., Rajulapati, C. R., Clark, M. P., and Lehner, F.: Robustness of CMIP6 historical global mean  
1010 temperature simulations: Trends, long-term persistence, autocorrelation, and distributional shape, *Earth's*  
1011 *Future*, 8, e2020EF001667, <https://doi.org/10.1029/2020EF001667>, 2020.

1012 Pascoe, C., Lawrence, B. N., Guilyardi, E., Juckes, M., and Taylor, K. E.: Documenting numerical experiments in  
1013 support of the Coupled Model Intercomparison Project Phase 6 (CMIP6), *Geosci. Model Dev.*, 13, 2149–  
1014 2167, <https://doi.org/10.5194/gmd-13-2149-2020>, 2020.

1015 Pendergrass, A. G., Gleckler, P. J., Leung, L. R., and Jakob, C.: Benchmarking simulated precipitation in earth system  
1016 models, *Bulletin of the American Meteorological Society*, 101, E814–E816, [https://doi.org/10.1175/bams-d-](https://doi.org/10.1175/bams-d-19-0318.1)  
1017 19-0318.1, 2020.

1018 Phillips, A. S., Deser, C., and Fasullo, J. T.: Evaluating modes of variability in climate models, *Eos, Transactions*  
1019 *American Geophysical Union*, 95, 453–455, <https://doi.org/10.1002/2014eo490002>, 2014.

1020 Planton, Y., Guilyardi, E., Wittenberg, A. T., Lee, J., Gleckler, P. J., Bayr, T., McGregor, S., McPhaden, M. J., Power,  
1021 S. B., Roehrig, R., Vialard, J., and Voltaire, A.: Evaluating Climate Models with the CLIVAR 2020 ENSO  
1022 Metrics Package, *Bulletin of the American Meteorological Society*, 102, E193–E217,  
1023 <https://doi.org/10.1175/bams-d-19-0337.1>, 2021.

1024 Potter, G. L., Bader, D. C., Riches, M., Bamzai, A. and Joseph, R.: Celebrating two decades of the Program for Climate  
1025 Model Diagnosis and Intercomparison. *Bulletin of the American Meteorological Society*, 92, 629–631,  
1026 <https://doi.org/10.1175/2011BAMS3018.1>, 2011.

1027 Qin, Y., Zelinka, M. D., and Klein, S. A.: On the Correspondence Between Atmosphere-Only and Coupled  
1028 Simulations for Radiative Feedbacks and Forcing From CO<sub>2</sub>, *Journal of Geophysical Research:*  
1029 *Atmospheres*, 127, <https://doi.org/10.1029/2021jd035460>, 2022.

1030 Randall, D.A., Wood, R.A., Bony, S., Colman, R., Fichet, T., Fyfe, J., Kattsov, V., Pitman, A., Shukla, J., Srinivasan,  
1031 J. and Stouffer, R.J.: Climate models and their evaluation. In *Climate change 2007: The physical science*  
1032 *basis. Contribution of Working Group I to the Fourth Assessment Report of the IPCC (FAR)*, 589–662,  
1033 Cambridge University Press, 2007.

1034 Randerson, J. T., Hoffman, F. M., Thornton, P. E., Mahowald, N. M., Lindsay, K., Lee, Y.-H., Nevison, C. D., Doney,  
1035 S. C., Bonan, G. B., Stöckli, R., Covey, C., Running, S. W., and Fung, I.: Systematic assessment of terrestrial



- 1036 biogeochemistry in coupled climate-carbon models, *Global Change Biology*, 15, 2462–2484,  
1037 <https://doi.org/10.1111/j.1365-2486.2009.01912.x>, 2009.
- 1038 Rasch, P. J., Xie, S., Ma, P.-L., Lin, W., Wang, H., Tang, Q., Burrows, S. M., Caldwell, P., Zhang, K., Easter, R. C.,  
1039 Cameron-Smith, P. J., Singh, B., Wan, H., Golaz, J.-C., Harrop, B. E., Roesler, E. L., Bacmeister, J. T.,  
1040 Larson, V. E., Evans, K. J., Qian, Y., Taylor, M. A., Leung, L. R., Zhang, Y., Brent, L., Branstetter, M. L.,  
1041 Hannay, C., Mahajan, S., Mametjanov, A., Neale, R., Richter, J. H., Yoon, J.-H., Zender, C. S., Bader, D. C.,  
1042 Flanner, M., Foucar, J. G., Jacob, R., Keen, N. D., Klein, S. A., Liu, X., Salinger, A. G., Shrivastava, M., and  
1043 Yang, Y.: An overview of the atmospheric component of the Energy Exascale Earth System model, *Journal*  
1044 *of Advances in Modeling Earth Systems*, 11, 2377–2411, <https://doi.org/10.1029/2019ms001629>, 2019.
- 1045 Reichler, T. and Kim, J.: How well do coupled models simulate today’s climate?, *Bulletin of the American*  
1046 *Meteorological Society*, 89, 303–312, <https://doi.org/10.1175/bams-89-3-303>, 2008.
- 1047 Righi, M., Andela, B., Eyring, V., Lauer, A., Predoi, V., Schlund, M., Vegas-Regidor, J., Bock, L., Brötz, B., De  
1048 Mora, L., Diblen, F., Dreyer, L., Drost, N., Earnshaw, P., Hassler, B., Koldunov, N., Little, B., Tomas, S. L.,  
1049 and Zimmermann, K.: Earth System Model Evaluation Tool (ESMValTool) v2.0 – technical overview,  
1050 *Geoscientific Model Development*, 13, 1179–1199, <https://doi.org/10.5194/gmd-13-1179-2020>, 2020.
- 1051 Sanderson, B. M. and Wehner, M. F.: Weighting strategy for the Fourth National Climate Assessment, in: *Climate*  
1052 *Science Special Report: Fourth National Climate Assessment, Volume I*, edited by Wuebbles, D. J., Fahey,  
1053 D. W., Hibbard, K. A., Dokken, D. J., Stewart, B. C., and Maycock, T.K., U.S. Global Change Research  
1054 Program, Washington, DC, USA, 436–442, <https://doi.org/10.7930/J06T0JS3>, 2017.
- 1055 Sanderson, B. M., Wehner, M., and Knutti, R.: Skill and independence weighting for multi-model assessments,  
1056 *Geoscientific Model Development*, 10, 2379–2395, <https://doi.org/10.5194/gmd-10-2379-2017>, 2017.
- 1057 Sherwood, S. C., Webb, M. J., Annan, J. D., Armour, K. C., Forster, P. M., Hargreaves, J. C., Hegerl, G. C., Klein, S.  
1058 A., Marvel, K., Rohling, E. J., Watanabe, M., Andrews, T., Braconnot, P., Bretherton, C. S., Foster, G. L.,  
1059 Hausfather, Z., Von Der Heydt, A. S., Knutti, R., Mauritsen, T., Norris, J. R., Proistosescu, C., Rugenstein,  
1060 M., Schmidt, G. A., Tokarska, K., and Zelinka, M. D.: An assessment of Earth’s climate sensitivity using  
1061 multiple lines of evidence, *Reviews of Geophysics*, 58, <https://doi.org/10.1029/2019rg000678>, 2020.
- 1062 Sillmann, J., Kharin, V. V., Zhang, X., Zwiers, F. W., and Bronaugh, D.: Climate extremes indices in the CMIP5  
1063 multimodel ensemble: Part 1. Model evaluation in the present climate, *Journal of Geophysical Research:*  
1064 *Atmospheres*, 118, 1716–1733, <https://doi.org/10.1002/jgrd.50203>, 2013.
- 1065 Sperber, K. R.: Madden-Julian variability in NCAR CAM2.0 and CCSM2.0, *Clim Dyn* 23, 259–278,  
1066 <https://doi.org/10.1007/s00382-004-0447-4>, 2004.
- 1067 Sperber, K. R., Annamalai, H., Kang, I.-S., Kitoh, A., Moise, A., Turner, A., Wang, B., and Zhou, T.: The Asian  
1068 summer monsoon: an intercomparison of CMIP5 vs. CMIP3 simulation of the late 20th century. *Clim Dyn*  
1069 41, 2711–2744, <https://doi.org/10.1007/s00382-012-1607-6>, 2013.
- 1070 Sperber K. R., Gualdi, S., Legutke, S., Gayler, V.: The Madden–Julian oscillation in ECHAM4 coupled and uncoupled  
1071 general circulation models, *Clim Dyn* 25, 117–140, <https://doi.org/10.1007/s00382-005-0026-3>, 2005.



1072 Srivastava, A., Grotjahn, R., and Ullrich, P. A.: Evaluation of historical CMIP6 model simulations of extreme  
1073 precipitation over contiguous US regions, *Weather and Climate Extremes*, 29, 100268,  
1074 <https://doi.org/10.1016/j.wace.2020.100268>, 2020.

1075 Steed, C. A., Shipman, G., Thornton, P., Ricciuto, D., Erickson, D. and Branstetter, M.: Practical application of parallel  
1076 coordinates for climate model analysis, *Procedia Computer Science*, 9, 877-886,  
1077 <https://doi.org/10.1016/j.procs.2012.04.094>, 2012.

1078 Stevens, B., Satoh, M., Auger, L., Biercamp, J., Bretherton, C. S., Chen, X., Düben, P., Judt, F., Khairoutdinov, M.,  
1079 Klocke, D., Kodama, C., Kornbluh, L., Lin, S.-J., Neumann, P., Putman, W. M., Röber, N., Shibuya, R.,  
1080 Vanniere, B., Vidale, P. L., Wedi, N., and Zhou, L.: DYAMOND: the DYnamics of the Atmospheric general  
1081 circulation Modeled On Non-hydrostatic Domains, *Progress in Earth and Planetary Science*, 6,  
1082 <https://doi.org/10.1186/s40645-019-0304-z>, 2019.

1083 Stoner, A. M. K., Hayhoe, K., and Wuebbles, D. J.: Assessing general circulation model simulations of atmospheric  
1084 teleconnection patterns, *Journal of Climate*, 22, 4348–4372, <https://doi.org/10.1175/2009jcli2577.1>, 2009.

1085 Sung, H. M., Kim, J., Shim, S., Seo, J., Kwon, S.-H., Sun, M.-A., Moon, H.-J., Lee, J., Lim, Y. C., Boo, K.-O., Kim,  
1086 Y., Lee, J., Lee, J., Kim, J.-S., Marzin, C., and Byun, Y.-H.: Climate change projection in the Twenty-First  
1087 Century simulated by NIMS-KMA CMIP6 model based on new GHGs concentration pathways, *Asia-pacific  
1088 Journal of Atmospheric Sciences*, 57, 851–862, <https://doi.org/10.1007/s13143-021-00225-6>, 2021.

1089 Tang, Q., Prather, M. J., Hsu, J., Ruiz, D. J., Cameron-Smith, P. J., Xie, S., and Golaz, J.-C.: Evaluation of the  
1090 interactive stratospheric ozone (O3v2) module in the E3SM version 1 Earth system model, *Geoscientific  
1091 Model Development*, 14, 1219–1236, <https://doi.org/10.5194/gmd-14-1219-2021>, 2021.

1092 Tang, S., Fast, J. D., Zhang, K., Hardin, J. C., Varble, A. C., Shilling, J. E., Mei, F., Zawadowicz, M. A., and Ma, P.-  
1093 L.: Earth System Model Aerosol–Cloud Diagnostics (ESMAC Diags) package, version 1: assessing E3SM  
1094 aerosol predictions using aircraft, ship, and surface measurements, *Geosci. Model Dev.*, 15, 4055–4076,  
1095 <https://doi.org/10.5194/gmd-15-4055-2022>, 2022.

1096 Tang, S., Varble, A. C., Fast, J. D., Zhang, K., Wu, P., Dong, X., Mei, F., Pekour, M., Hardin, J. C., and Ma, P.-L.:  
1097 Earth System Model Aerosol–Cloud Diagnostics (ESMAC Diags) package, version 2: assessing aerosols,  
1098 clouds, and aerosol–cloud interactions via field campaign and long-term observations, *Geosci. Model Dev.*,  
1099 16, 6355–6376, <https://doi.org/10.5194/gmd-16-6355-2023>, 2023.

1100 Taylor, K. E.: Truly Conserving with Conservative Remapping Methods, *Geosci. Model Dev. Discuss.* [preprint],  
1101 <https://doi.org/10.5194/gmd-2023-177>, in review, 2023.

1102 Taylor, K. E.: Summarizing multiple aspects of model performance in a single diagram, *Journal of Geophysical  
1103 Research*, 106, 7183–7192, <https://doi.org/10.1029/2000jd900719>, 2001.

1104 Taylor, K. E., Stouffer, R. J., and Meehl, G. A.: An overview of CMIP5 and the experiment design, *Bulletin of the  
1105 American Meteorological Society*, 93, 485–498, <https://doi.org/10.1175/bams-d-11-00094.1>, 2012.

1106 Teixeira, J., Waliser, D. E., Ferraro, R., Gleckler, P. J., Lee, T., and Potter, G. L.: Satellite observations for CMIP5:  
1107 The Genesis of OBS4MIPs, *Bulletin of the American Meteorological Society*, 95, 1329–1334,  
1108 <https://doi.org/10.1175/bams-d-12-00204.1>, 2014.



- 1109 Tian, B., and Dong, X.: The Double-ITCZ Bias in CMIP3, CMIP5, and CMIP6 Models Based on Annual Mean  
1110 Precipitation, *Geophysical Research Letters*, 47, e2020GL087232, <https://doi.org/10.1029/2020GL087232>,  
1111 2020
- 1112 Ullrich, P. A. and Zarzycki, C. M.: TempestExtremes: a framework for scale-insensitive pointwise feature tracking on  
1113 unstructured grids, *Geoscientific Model Development*, 10, 1069–1090, [https://doi.org/10.5194/gmd-10-](https://doi.org/10.5194/gmd-10-1069-2017)  
1114 1069-2017, 2017.
- 1115 Ullrich, P. A., Zarzycki, C. M., McClenny, E., Pinheiro, M. C., Stansfield, A. M., and Reed, K. A.: TempestExtremes  
1116 v2.1: a community framework for feature detection, tracking, and analysis in large datasets, *Geoscientific*  
1117 *Model Development*, 14, 5023–5048, <https://doi.org/10.5194/gmd-14-5023-2021>, 2021.
- 1118 U.S. Department of Energy (DOE): Benchmarking Simulated Precipitation in Earth System Models Workshop Report,  
1119 DOE/SC-0203, U.S. Department of Energy Office of Science, Biological and Environmental Research (BER)  
1120 Program. Germantown, Maryland, USA. 2020.
- 1121 Vo, T., Po-Chedley, P., Boutte, J., Zhang, C., Lee, J., Gleckler, P., Durack, P., Taylor, K., and Golaz, J.-C.: Xarray  
1122 Climate Data Analysis Tools (xCDAT): A Python Package for Simple and Robust Analysis of Climate Data,  
1123 The 103rd AMS Annual Meeting, Abstract, 2023.
- 1124 Waliser, D. E., Gleckler, P. J., Ferraro, R., Taylor, K. E., Ames, S., Biard, J., Bosilovich, M. G., Brown, O. B., Chepfer,  
1125 H., Cinquini, L., Durack, P. J., Eyring, V., Mathieu, P.-P., Lee, T., Pinnock, S., Potter, G. L., Rixen, M.,  
1126 Saunders, R., Schulz, J. B., Thépaut, J.-N., and Tuma, M.: Observations for Model Intercomparison Project  
1127 (Obs4MIPs): status for CMIP6, *Geoscientific Model Development*, 13, 2945–2958,  
1128 <https://doi.org/10.5194/gmd-13-2945-2020>, 2020.
- 1129 Waliser, D. E., Sperber, K. R., Hendon, H. H., Kim, D., Maloney, E. D., Wheeler, M. C., Weickmann, K. M., Zhang,  
1130 C., Donner, L. J., Gottschalck, J., Higgins, W., Kang, I. S., Legler, D. M., Moncrieff, M. W., Schubert, S. D.,  
1131 Stern, W., Vitart, F., Wang, B., Wang, W., and Woolnough, S. J.: MJO Simulation Diagnostics, *Journal of*  
1132 *Climate*, 22, 3006–3030, <https://doi.org/10.1175/2008jcli2731.1>, 2009.
- 1133 Wang, J., Liu, X., Shen, H. W. and Lin, G.: Multi-resolution climate ensemble parameter analysis with nested parallel  
1134 coordinates plots, *IEEE Transactions on Visualization and Computer Graphics*, 23, 81–90,  
1135 <https://doi.org/10.1109/TVCG.2016.2598830>, 2017.
- 1136 Wehner, M., Gleckler, P. J., and Lee, J.: Characterization of long period return values of extreme daily temperature  
1137 and precipitation in the CMIP6 models: Part 1, model evaluation, *Weather and Climate Extremes*, 30,  
1138 100283, <https://doi.org/10.1016/j.wace.2020.100283>, 2020.
- 1139 Wehner, M., Lee, J., Risser, M. D., Ullrich, P. A., Gleckler, P. J., and Collins, W. D.: Evaluation of extreme sub-daily  
1140 precipitation in high-resolution global climate model simulations, *Philosophical Transactions of the Royal*  
1141 *Society A*, 379, 20190545, <https://doi.org/10.1098/rsta.2019.0545>, 2021.
- 1142 Whitehall, K., Mattmann, C., Waliser, D., Kim, J., Goodale, C., Hart, A., Ramirez, P., Zimdars, P., Crichton, D.,  
1143 Jenkins, G., Jones, C., Asrar, G., and Hewitson, B.: Building Model Evaluation and Decision Support  
1144 Capacity for CORDEX, *WMO Bulletin*, 61, available at:





- 1145 [https://public.wmo.int/en/resources/bulletin/building-model-evaluation-and-decision-support-capacity-](https://public.wmo.int/en/resources/bulletin/building-model-evaluation-and-decision-support-capacity-cordex)  
1146 [cordex](https://public.wmo.int/en/resources/bulletin/building-model-evaluation-and-decision-support-capacity-cordex) (last access date: 14 September 2023), 2012.
- 1147 Williams, D. N.: Visualization and analysis tools for ultrascale climate data, *Eos, Transactions American Geophysical*  
1148 *Union*, 95, 377–378, <https://doi.org/10.1002/2014eo420002>, 2014.
- 1149 Williams, D. N., Balaji, V., Cinquini, L., Denvil, S., Duffy, D. Q., Evans, B., Ferraro, R., Hansen, R., Lautenschlager,  
1150 M., and Trenham, C.: A global repository for Planet-Sized experiments and observations, *Bulletin of the*  
1151 *American Meteorological Society*, 97, 803–816, <https://doi.org/10.1175/bams-d-15-00132.1>, 2016.
- 1152 Williams, D. N., Doutriaux, C., Drach, R., and McCoy, R.: The Flexible Climate Data Analysis Tools (CDAT) for  
1153 Multi-model Climate Simulation Data, *IEEE International Conference on Data Mining Workshops*, 254–261,  
1154 <https://doi.org/10.1109/icdmw.2009.64>, 2009.
- 1155 Wong, P. C., Shen, H. W., Leung, R., Hagos, S., Lee, T. Y., Tong, X. and Lu, K.: Visual analytics of large-scale  
1156 climate model data, in: 2014 IEEE 4th Symposium on Large Data Analysis and Visualization (LDAV), 85-  
1157 92, <https://doi.org/10.1109/LDAV.2014.7013208>, 2014.
- 1158 Xie, P., Joyce, R., Wu, S., Yoo, S.H., Yarosh, Y., Sun, F. and Lin, R.: Reprocessed, bias-corrected CMORPH global  
1159 high-resolution precipitation estimates from 1998, *Journal of Hydrometeorology*, 18, 1617-1641, 2017.
- 1160 Xue, Z. and Ullrich, P. A.: A Comprehensive Intermediate-Term Drought Evaluation System and Evaluation of  
1161 Climate Data Products over the Conterminous United States, *Journal of Hydrometeorology*,  
1162 <https://doi.org/10.1175/jhm-d-20-0314.1>, 2021.
- 1163 Young, A. H., Knapp, K. R., Inamdar, A. K., Hankins, W., and Rossow, W. B.: The International Satellite Cloud  
1164 Climatology Project H-Series climate data record product, *Earth System Science Data*, 10, 583–593,  
1165 <https://doi.org/10.5194/essd-10-583-2018>, 2018.
- 1166 Zelinka, M. D., Klein, S. A., Qin, Y., and Myers, T. A.: Evaluating climate models’ cloud feedbacks against expert  
1167 judgment, *Journal of Geophysical Research: Atmospheres*, 127, <https://doi.org/10.1029/2021jd035198>,  
1168 2022.
- 1169 Zelinka, M. D., Myers, T. A., McCoy, D. T., Po-Chedley, S., Caldwell, P. M., Ceppi, P., Klein, S. A., and Taylor, K.  
1170 E.: Causes of higher climate sensitivity in CMIP6 models, *Geophysical Research Letters*, 47,  
1171 e2019GL085782, <https://doi.org/10.1029/2019GL085782>, 2020.
- 1172 Zhang, C., Golaz, J.-C., Forsyth, R., Vo, T., Xie, S., Shaheen, Z., Potter, G. L., Asay-Davis, X. S., Zender, C. S., Lin,  
1173 W., Chen, C.-C., Terai, C. R., Mahajan, S., Zhou, T., Balaguru, K., Tang, Q., Tao, C., Zhang, Y.,  
1174 Emmenegger, T., Burrows, S., and Ullrich, P. A.: The E3SM Diagnostics Package (E3SM Diags v2.7): a  
1175 Python-based diagnostics package for Earth system model evaluation, *Geosci. Model Dev.*, 15, 9031–9056,  
1176 <https://doi.org/10.5194/gmd-15-9031-2022>, 2022.
- 1177 Zhang, C. and Hendon, H. H.: Propagating and standing components of the intraseasonal oscillation in tropical  
1178 convection, *Journal of the Atmospheric Sciences*, 54, 741–752, [https://doi.org/10.1175/1520-0469\(1997\)054](https://doi.org/10.1175/1520-0469(1997)054), 1997.
- 1180 Zhang, C., Xie, S., Klein, S. A., Ma, H. Y., Tang, S., Van Weverberg, K., Morcrette, C. J. and Petch, J.: CAUSES:  
1181 Diagnosis of the summertime warm bias in CMIP5 climate models at the ARM Southern Great Plains site.

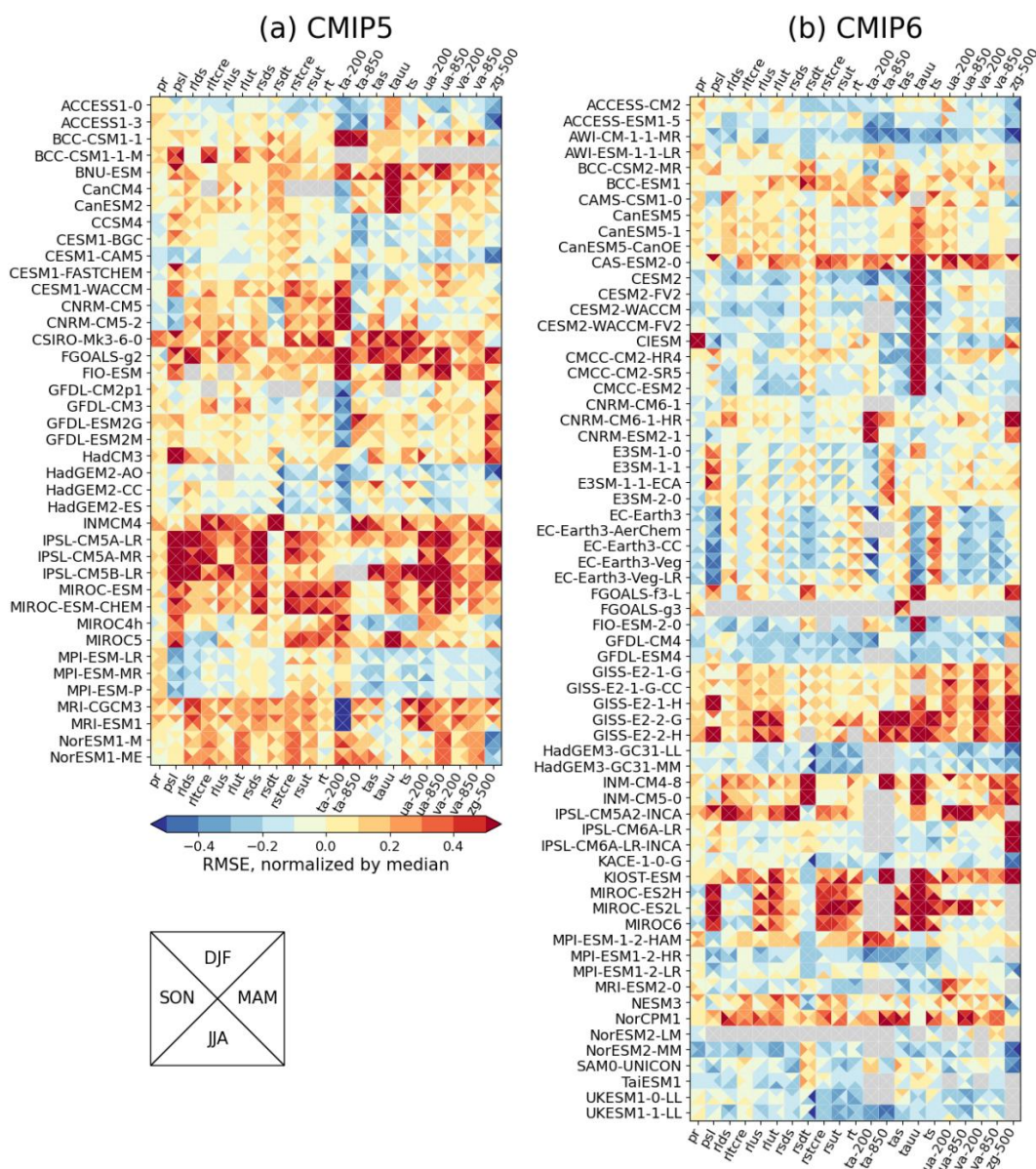


- 1182           Journal of Geophysical Research: Atmospheres, 123, 2968-2992, <https://doi.org/10.1002/2017JD027200>,  
1183           2018.
- 1184   Zhang, C., Xie, S., Tao, C., Tang, S., Emmenegger, T., Neelin, J. D., Schiro, K. A., Lin, W. and Shaheen, Z.: The  
1185           ARM data-oriented metrics and diagnostics package for climate models: A new tool for evaluating climate  
1186           models with field data, <https://doi.org/10.1175/BAMS-D-19-0282.1>, Bulletin of the American  
1187           Meteorological Society, 101, E1619-E1627, 2020.
- 1188   Zhang, M.-Z., Xu, Z., Han, Y., and Guo, W.: An improved multivariable integrated evaluation method and tool  
1189           (MVIETool) v1.0 for multimodel intercomparison, Geoscientific Model Development, 14, 3079–3094,  
1190           <https://doi.org/10.5194/gmd-14-3079-2021>, 2021.
- 1191   Zhao, B., Lin, P., Hu, A., Liu, H., Ding, M., Yu, Z., and Yu, Y.: Uncertainty in Atlantic Multidecadal Oscillation  
1192           derived from different observed datasets and their possible causes, Frontiers in Marine Science, 9,  
1193           <https://doi.org/10.3389/fmars.2022.1007646>, 2022.
- 1194   Zhao, M., Golaz, J.-C., Held, I. M., Guo, H., Balaji, V., Benson, R., Chen, J. H., Chen, X., Donner, L. J., Dunne, J.,  
1195           Dunne, K. A., Durachta, J., Fan, S.-M., Freidenreich, S. M., Garner, S. T., Ginoux, P., Harris, L., Horowitz,  
1196           L. W., Krasting, J. P., Langenhorst, A. R., Zhi, L., Lin, P., Lin, S. J., Malyshev, S., Mason, E., Milly, P. C.  
1197           D., Ming, Y., Naik, V., Paulot, F., Paynter, D., Phillipps, P. J., Radhakrishnan, A., Ramaswamy, V.,  
1198           Robinson, T., Schwarzkopf, D., Seman, C. J., Shevliakova, E., Shen, Z., Shin, H. H., Silvers, L. G., Wilson,  
1199           J. R., Winton, M., Wittenberg, A. T., Wyman, B., and Xiang, B.: The GFDL Global Atmosphere and Land  
1200           Model AM4.0/LM4.0: 1. Simulation characteristics with prescribed SSTs, Journal of Advances in Modeling  
1201           Earth Systems, 10, 691–734, <https://doi.org/10.1002/2017ms001208>, 2018.  
1202



1203 **Table 1.** List of variables and observation datasets used as reference datasets for the PMP's  
 1204 mean climate evaluation in this paper (Section 3.1 and Figs. 1-2). A ditto mark (") indicates the  
 1205 same as above.  
 1206

Variable	Variable full name	Product	Reference
ps	Precipitation	GPCP-2-3	Adler et al. (2018)
psl	Sea level pressure	ERA-5	Hersbach et al. (2020)
rlds	Surface Downwelling Longwave Radiation	CERES-EBAF-4-1	Loeb et al. (2018)
rltcre	Longwave cloud radiative effect	"	
rlus	Surface Upwelling Longwave Radiation	"	
rlut	Upwelling longwave at the top of atmosphere	"	
rsds	Surface Downwelling Shortwave Radiation	"	
rsdt	TOA Incident Shortwave Radiation	"	
rstcre	Shortwave cloud radiative effect	"	
rsut	Upwelling shortwave at the top of atmosphere	"	
rt	Net radiative flux	"	
ta-200, ta-850	Air temperature at 850 and 200 hPa	ERA-5	Hersbach et al. (2020)
tas	2-m air temperature	"	
tauu	Surface zonal wind stress	ERA-INT	Dee et al. (2011)
ts	Surface temperature	ERA-5	Hersbach et al. (2020)
ua-200, ua-850	Zonal wind component at 850 and 200 hPa	"	
va-200, va-850	Meridional wind component at 850 and 200 hPa	"	
zg-500	Geopotential height at 500 hPa	"	

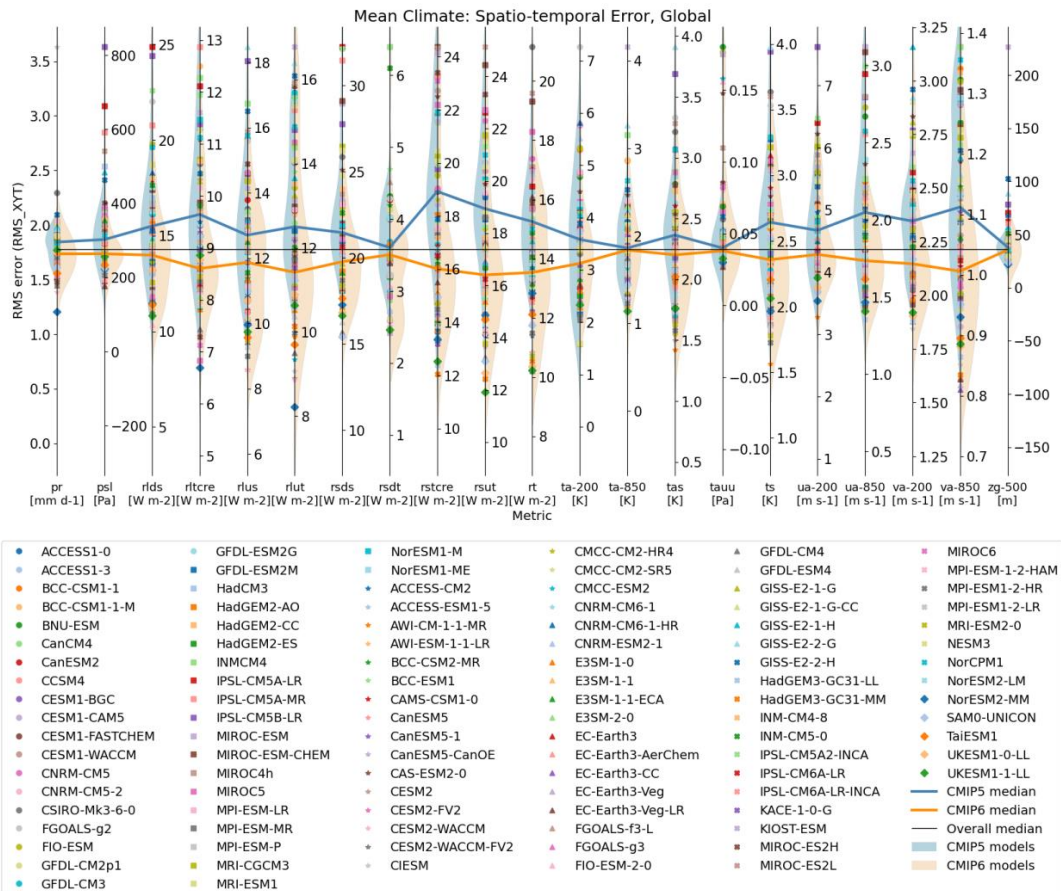


1207  
 1208 **Figure 1.** Portrait plot for spatial RMSE (uncentered) of global seasonal climatologies for (a)  
 1209 CMIP5 (models ACCESS1-0 to NorESM1-ME on the ordinate) and (b) CMIP6 (models  
 1210 ACCESS-CM2 to UKESM1-1-LL on the ordinate) for 1981-2005 epoch. The RMSE of each  
 1211 variable is normalized by the median RMSE of all CMIP5 and 6 models. A result of 0.2 (-0.2) is  
 1212 indicative of an error that is 20% greater (lesser) than the median RMSE across all models.  
 1213 Models in each group are sorted in alphabetical order. Full names of variable names on the  
 1214 abscissa and their reference datasets can be found in Table 1. Detailed information for models  
 1215 can be found at the *Earth System Documentation* (ES-DOC, <https://search.es-doc.org/>; Pascoe

<https://doi.org/10.5194/egusphere-2023-2720>  
Preprint. Discussion started: 24 November 2023  
© Author(s) 2023. CC BY 4.0 License.

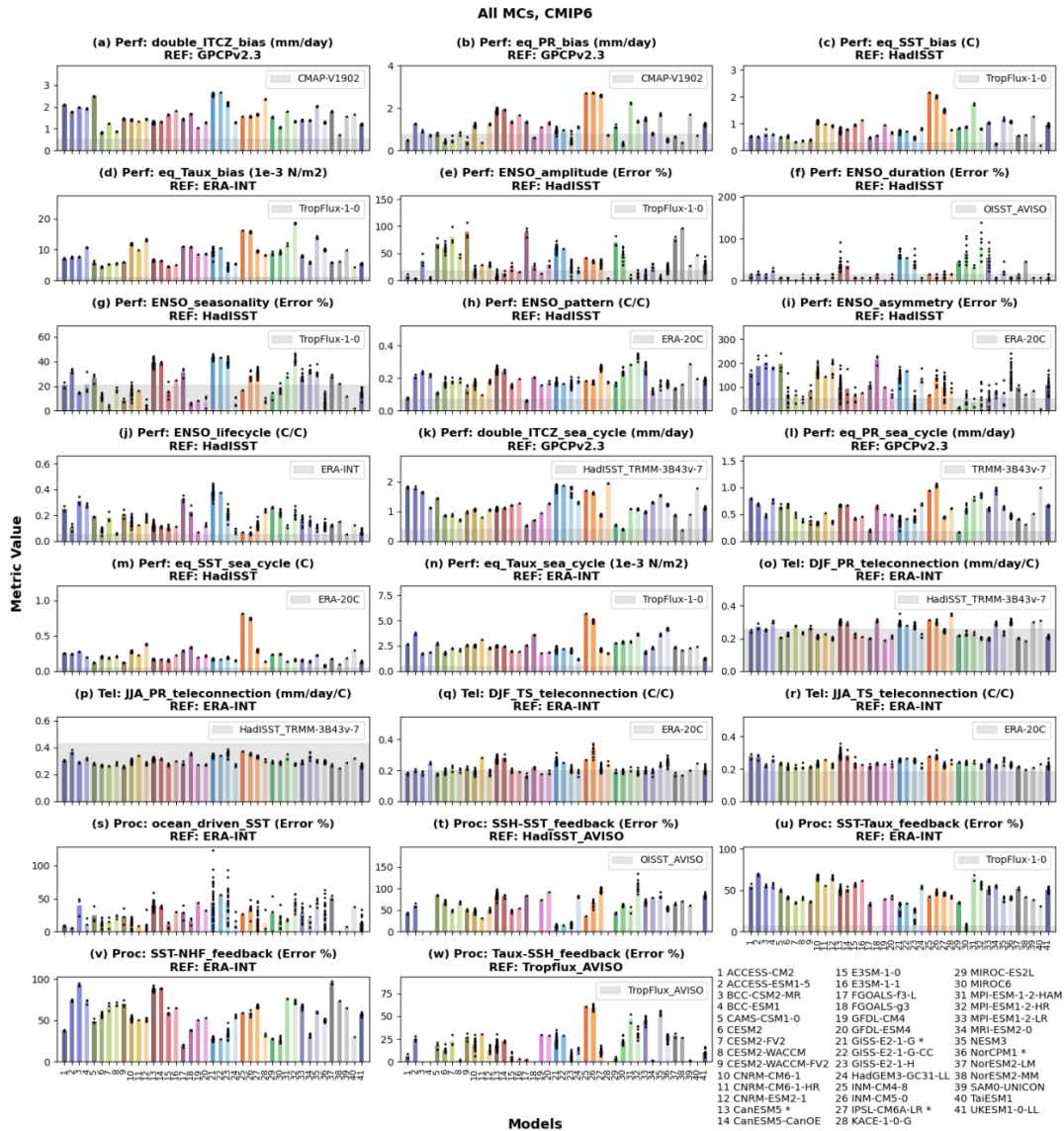


1216 et al., 2020). The interactive version of the Portrait plot in this figure is available on the PMP  
1217 result pages on the PCMDI website ([https://pcmdi.llnl.gov/metrics/mean\\_clim/](https://pcmdi.llnl.gov/metrics/mean_clim/)).



1218  
 1219  
 1220  
 1221  
 1222  
 1223  
 1224  
 1225  
 1226  
 1227  
 1228  
 1229  
 1230

**Figure 2.** Parallel Coordinate Plot for spatio-temporal RMSE (Gleckler et al., 2008) from mean climate evaluation. Each vertical axis represents a different variable. Results from each model are displayed as symbols. Middle of each vertical axis is aligned with the median statistic of all CMIP5 and CMIP6 models. The cross-generation model distributions of model performance are shaded on the left (CMIP5, blue) and right (CMIP6, orange) sides of each axis. Also, medians from CMIP5 (blue) and CMIP6 (orange) model groups are highlighted as lines. Full names for model variables on the abscissa and their reference datasets can be found in Table 1. Time epoch used for this analysis is 1981-2005. Detailed information for models can be found at the *Earth System Documentation* (ES-DOC, <https://search.es-doc.org/>; Pascoe et al., 2020). The interactive version of the Portrait plot in this figure is available on the PMP result pages on the PCMDI website ([https://pcmdi.llnl.gov/metrics/mean\\_clim/](https://pcmdi.llnl.gov/metrics/mean_clim/)).



1231  
 1232  
 1233  
 1234  
 1235  
 1236  
 1237  
 1238  
 1239  
 1240  
 1241

**Figure 3.** Application of ENSO metrics to CMIP6 models. Model names with an asterisk (\*) indicate that 10 or more ensemble members were used in this analysis. Dots indicate metric values from individual ensemble members while bars indicate the average of metric values across the ensemble members. Bars colored for easier identification of model names at the bottom of the figure. Metrics were grouped into three *Metric Collections*: (a-n) ENSO Performance, (o-r) ENSO Teleconnections, and (s-w) ENSO processes. Names of individual metrics and default reference datasets being used are noted on top of each panel, and observational uncertainty by applying the metrics for alternative reference datasets noted on the upper right of each panel is shown as gray-shaded. Detailed descriptions for each metric can be found at [https://github.com/CLIVAR-PRP/ENSO\\_metrics/wiki](https://github.com/CLIVAR-PRP/ENSO_metrics/wiki).

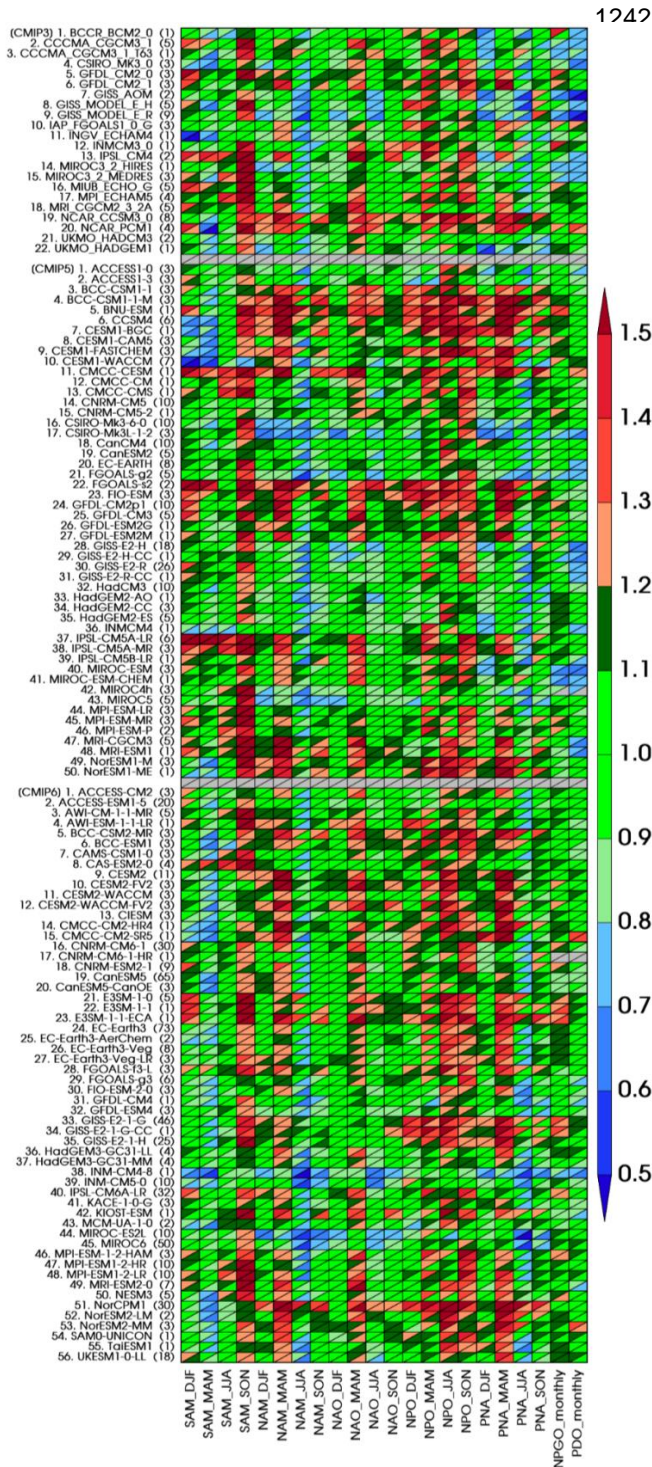
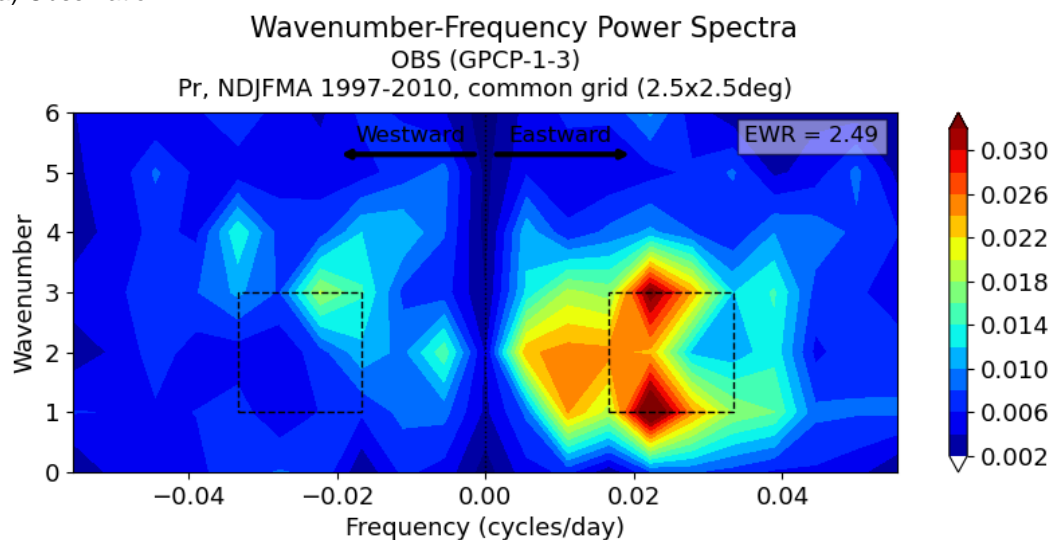


**Figure 4.** Portrait plots of the amplitude of extratropical modes of variability simulated by CMIP3, 5, and 6 models in their historical or equivalent simulations, as gauged by the ratio of spatiotemporal standard deviations of the model and observed PCs, obtained using the CBF method in the PMP. Columns (horizontal axis) are for mode and season, and rows (vertical axis) are for models from CMIP3 (top), CMIP5 (middle), and CMIP6 (bottom), separated by rows of gray boxes. For sea level pressure–based modes (SAM, NAM, NAO, NPO, and PNA) in the upper-left hand triangle the model results are shown relative to NOAA-20CR whereas in the lower-right triangle, the model results are shown relative to the ERA-20C. For SST-based modes (NPGO and PDO), results are shown relative to HadISSTv1.1 (upper-left triangle) and HadISSTv2.1 (lower-right triangle). Numbers in parentheses following model names indicate the number of ensemble members for the model. Metrics for individual ensemble members were averaged for each model. The figure is adapted from Lee et al. 2021b.

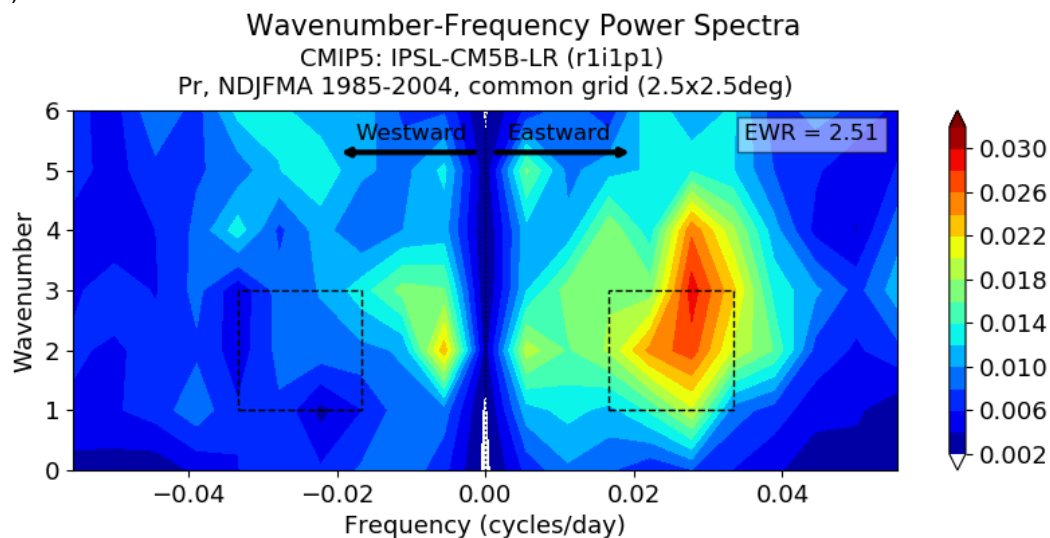




1281  
1282 (a) Observation

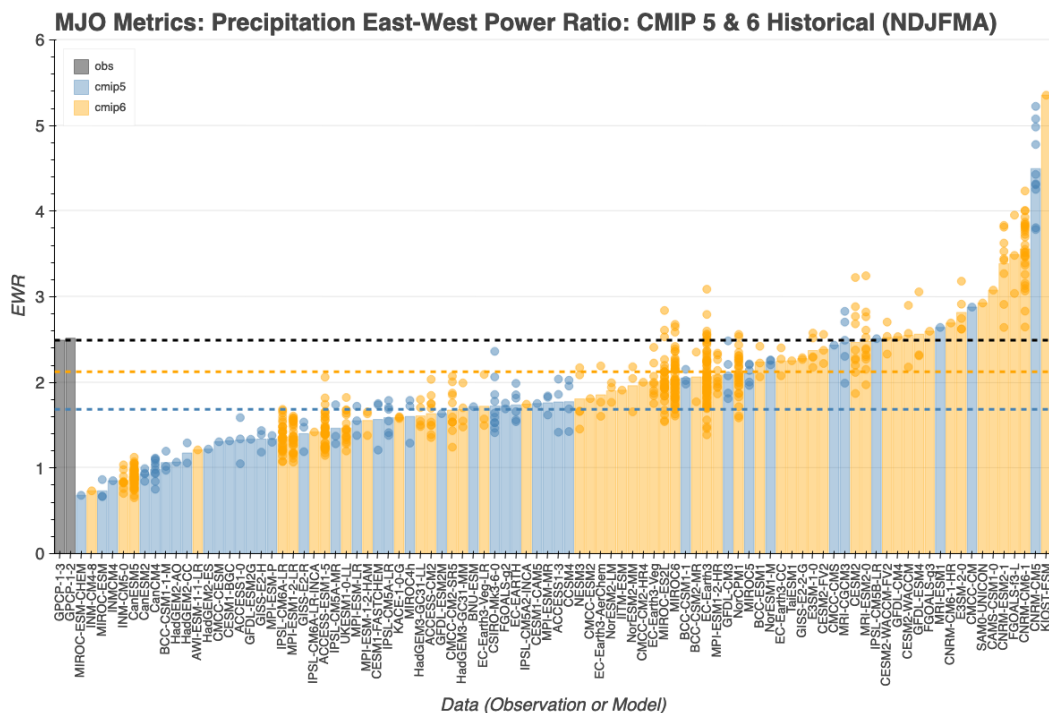


1283  
1284 (b) Model



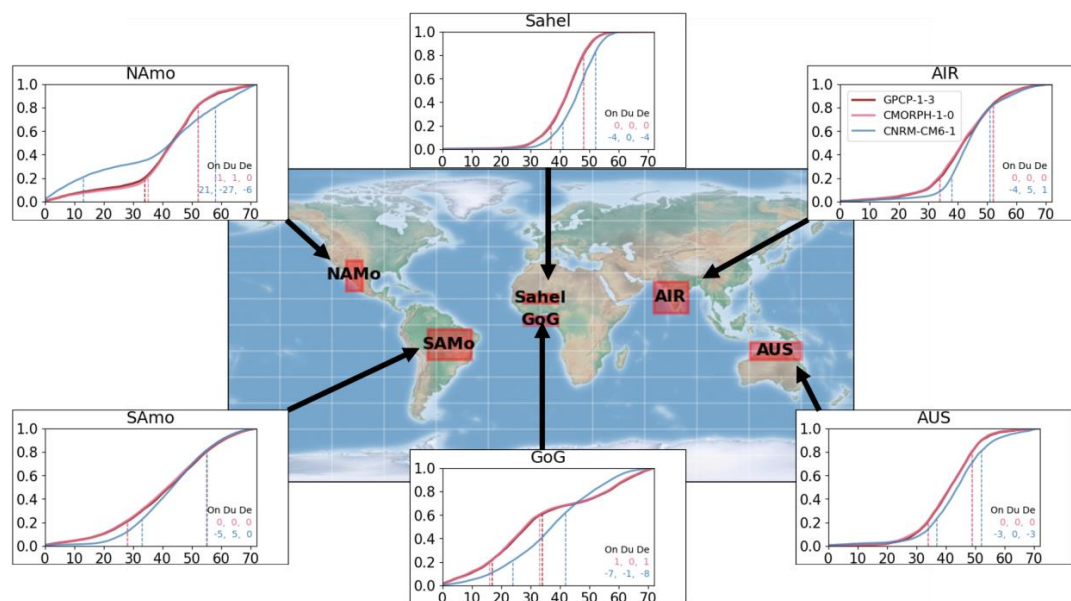
1285  
1286  
1287  
1288  
1289  
1290  
1291  
1292  
1293

**Figure 5.** MJO EWR diagnostics – wavenumber-frequency power spectra – from (a) GPCP v1.3 (Huffman et al., 2001) and (b) IPSL-CM5B-LR model of CMIP5. The EWR is defined as the ratio of eastward power (averaged in the box on the right) to westward power (averaged in the box on the left) from the 2-dimensional wavenumber-frequency power spectra of daily 10°S–10°N averaged precipitation in November to April (shaded,  $\text{mm}^2 \text{day}^{-2}$ ). Power spectra are calculated for each year and then averaged over all years of data. The units of power spectra for the precipitation is  $\text{mm}^2 \text{day}^{-2}$  per frequency interval per wavenumber interval.



1294  
 1295  
 1296  
 1297  
 1298  
 1299  
 1300  
 1301  
 1302  
 1303  
 1304

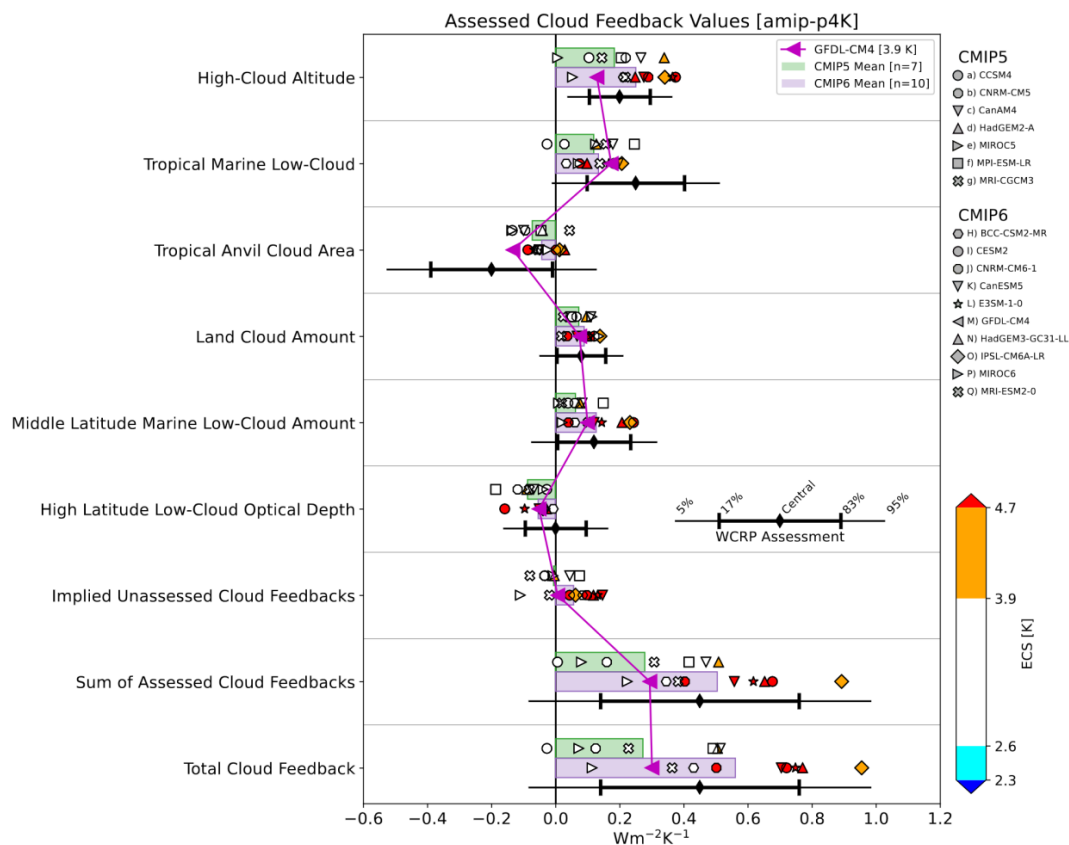
**Figure 6.** MJO EWR from CMIP5 and CMIP6 models, models in two different groups (CMIP5: blue, CMIP6: orange) are sorted by the value of the metric and compared to two observation datasets (purple, GPCP v1.2 and v1.3; Huffman et al., 2001). Horizontal dashed lines indicate EWR from the default primary reference observation (i.e., GPCP v1.3, black), averages of CMIP5 and CMIP6 models. The interactive plot is available at <https://pcmdi.llnl.gov/research/metrics/mjo/> where the horizontal axis can be resorted by CMIP group or model names as well. Hover mouse over boxes will show tooltips for metric values and a preview of dive-down plots that are shown in Figure 5.



1305  
1306 **Figure 7.** Demonstration of the monsoon metrics obtained from observation datasets (GPCP  
1307 v1.3 and CMORPH v1.0 (Joyce et al., 2004; Xie et al., 2017)) and a CMIP6 model's Historical  
1308 simulation conducted using CNRM-CM6-1. The results are obtained for monsoon regions: All-  
1309 India Rainfall (AIR), Sahel, Gulf of Guinea (GoG), North American Monsoon (NAM), South  
1310 American Monsoon (SAM), and Northern Australia (AUS). The regions are defined in Sperber  
1311 and Annamalai (2014). Metrics for onset (On), Duration (Du), and Decay (De) derived as  
1312 differences to the default observation (GPCP v1.3) in pentad indices (observation minus model)  
1313 are shown at lower right of each panel. Pentad indices for onset and decay of each region are  
1314 also shown as vertical lines.



1315

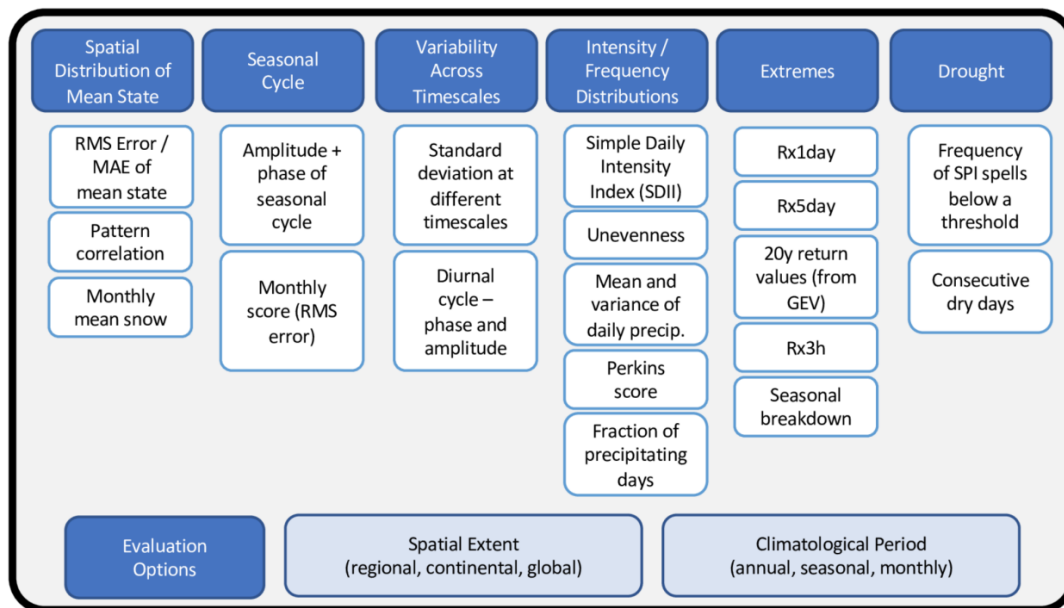


1316  
 1317  
 1318  
 1319  
 1320  
 1321  
 1322

**Figure 8.** Cloud feedback components estimated in amip-p4K simulations from CMIP5 and CMIP6 models. Symbols indicate individual model values, while horizontal bars indicate multi-model means. Each model is color-coded by its ECS, with color boundaries corresponding to the likely and very likely ranges of ECS as determined in Sherwood et al (2020). Each component's expert-assessed likely and very likely confidence intervals are indicated with black error bars. An illustrative model (GFDL-CM4) is highlighted.

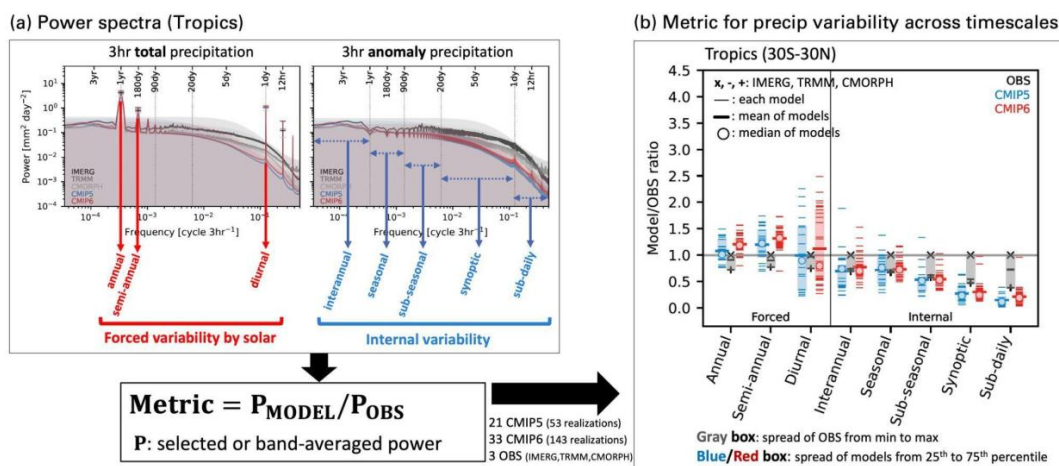


1323



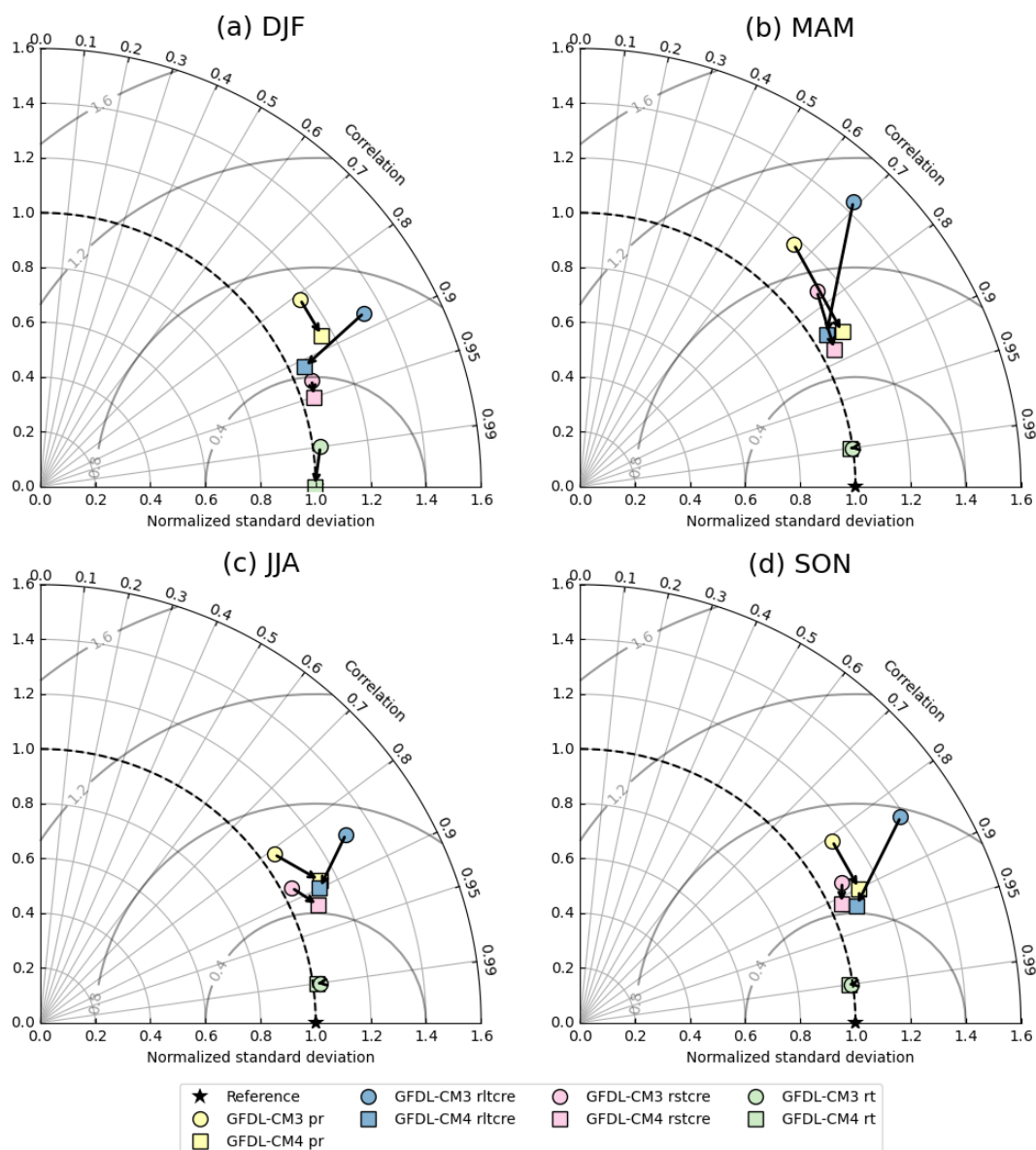
1324  
 1325  
 1326  
 1327  
 1328  
 1329  
 1330

**Figure 9.** Proposed suite of baseline metrics for simulated precipitation benchmarking (figure reprinted from workshop report; US DOE, 2020).

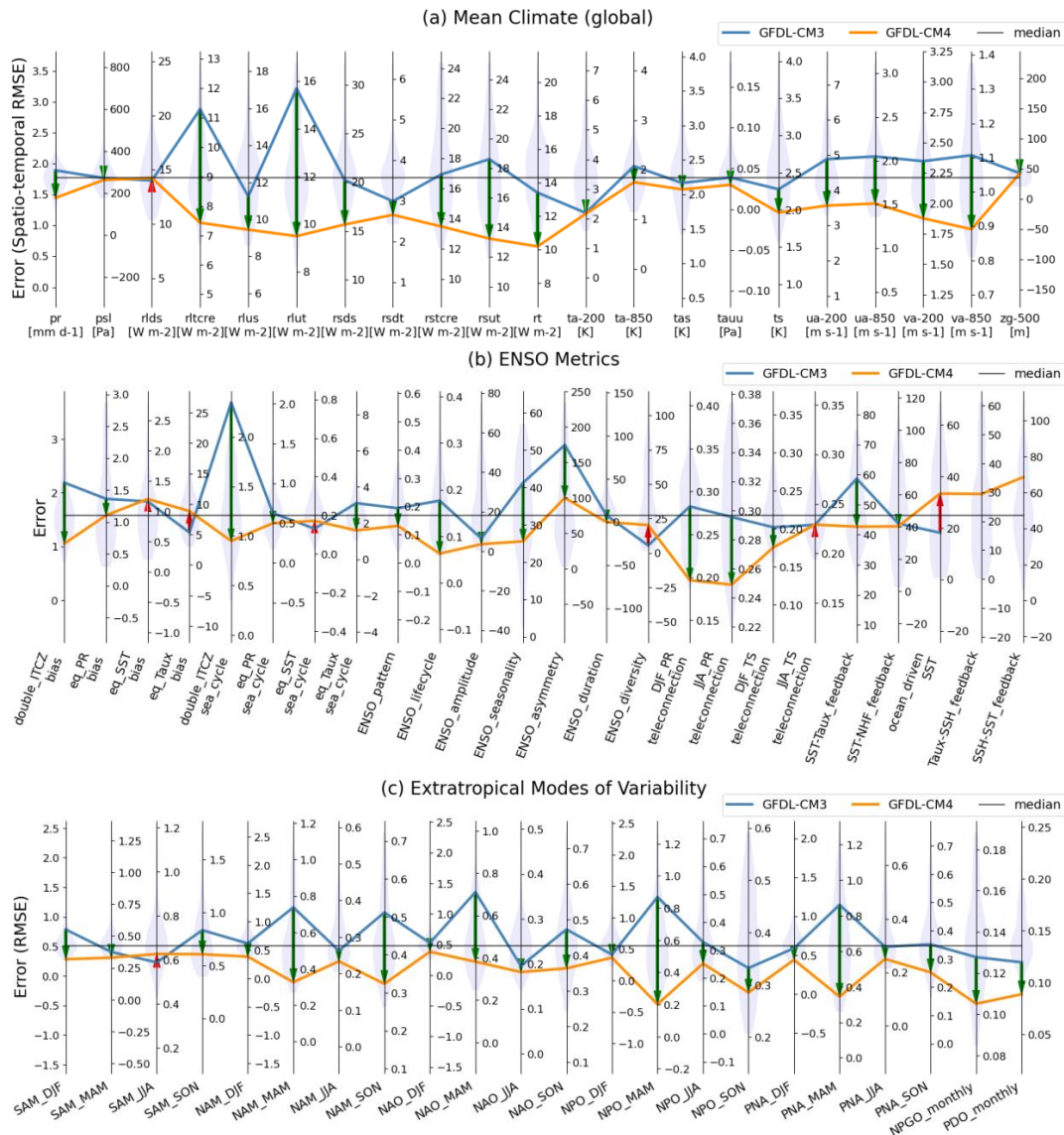


1331  
 1332  
 1333  
 1334  
 1335  
 1336  
 1337  
 1338  
 1339  
 1340  
 1341  
 1342  
 1343  
 1344  
 1345

**Figure 10.** Example (a) an underlying diagnostic and (b) its resulting metrics for precipitation variability across timescales. (a) Power spectra of 3-hourly total (left) and anomaly (right) precipitation from IMERG (black), TRMM (gray), CMORPH (silver), CMIP5 (blue), and CMIP6 (red) averaged over the tropics (30°S-30°N). The colored shading indicates the 95% confidence interval for each observational product and for the CMIP5 and CMIP6 means. (b) Metrics for forced and internal precipitation variability based on power spectra. The reference observational product displayed is GPM IMERG (Huffman et al., 2015). The gray boxes represent the spread of the three observational products (“X” for IMERG, “-” for TRMM, and “+” for CMORPH) from the minimum to maximum values. Blue and red boxes indicate the 25th to the 75th percentile of CMIP models as a measure of spread. Individual models are shown as thin dashes, the multimodel mean as a thick dash, and the multimodel median as an open circle. Details for the diagnostics and metrics are described in Ahn et al. (2022).



1346  
 1347 **Figure 11.** Taylor Diagram contrasting performance of an ESM in their two different versions  
 1348 (i.e., GFDL-CM3 from CMIP5 and GFDL-CM4 from CMIP6) in its Historical simulation for  
 1349 multiple variables (precipitation [pr], longwave cloud radiative effect [rltcre], shortwave cloud  
 1350 radiative effect [rstcre], and total radiation flux [rt]) in their climatology over the globe for (a) DJF,  
 1351 (b) MAM, (c) JJA and (d) SON seasons. The arrow is directed toward the newer version of the  
 1352 model from the older version (i.e., GFDL-CM3 → GFDL-CM4).



1353

1354

1355

1356

1357

1358

1359

1360

1361

1362

1363

1364

**Figure 12.** Parallel Coordinate Plot contrasting performance of two different versions of the GFDL model (i.e., GFDL-CM3 from CMIP5 and GFDL-CM4 from CMIP6) in their Historical experiment for errors from (a) mean climate, (b) ENSO, and (c) extratropical modes of variability. Considering lower indicates better, Improvement (degradation) in the later version of the model is highlighted as a downward green (upward red) arrow between lines. Middle of each vertical axis is set to the median of the group of benchmarking models (i.e., CMIP5 and CMIP6), with the axis range stretched to maximum distance to either minimum or maximum from the median for visual consistency. The inter-model distributions of model performance are shown as shaded violin plots along each vertical axis.